ELSEVIER

Wave Motion 35 (2002) 107–124

WAVE MOTION

www.elsevier.com/locate/wavemoti

Capillary–gravity wave transport over spatially random drift

Guillaume Bal [a], Tom Chou [b,*]

[a] *Department of Mathematics, University of Chicago, Chicago, IL 60637, USA*
[b] *Department of Biomathematics, UCLA, Los Angeles, CA 90095-1766, USA*

Received 18 October 2000; accepted 5 February 2001

Abstract

We derive transport equations for the propagation of water wave action in the presence of subsurface random flows. Using the Wigner distribution $\boldsymbol{W}(\boldsymbol{x}, \boldsymbol{k}, t)$ to represent the envelope of the wave amplitude at position $\boldsymbol{x}$, time t contained in high frequency waves with wave vector $\boldsymbol{k}/\varepsilon$ (where ε is a small parameter compared to a characteristic distance of propagation), we describe surface wave transport over flows consisting of two length scales; one varying slowly on the wavelength scale, the other varying on a scale comparable to the wavelength. Both static underlying flows and time-varying underlying flows are considered. The spatially rapidly varying but weak surface flows augment the characteristic equations with scattering terms that are explicit functions of the correlations of the random surface currents. These scattering terms depend parametrically on the magnitudes and directions of the smoothly varying drift and are shown to give rise to a Doppler-coupled scattering mechanism. Conservation of wave action (CWA), typically derived for drift varying over long distances, is extended to systems with flow that varies on small length scales of order the surface wavelength. Our results provide a formal set of equations to analyze transport of surface wave action, intensity, energy, and wave scattering as a function of the smoothly varying drifts and the correlation functions of the random, highly oscillating surface flows.

Keywords: Water waves; Transport; Drift

1. Introduction

Surface flows modify the free surface boundary conditions that determine the dispersion for propagating water waves. The effects of smoothly varying (compared to the wavelength) currents on water wave dynamics have been analyzed using ray theory [1,2] and the principle of conservation of wave action (CWA) (cf. [3–7] and references within). These studies and many others have largely focused on the linear and nonlinear dynamics of gravity waves propagating over even larger scale spatially varying drifts [8]. Water waves can also scatter from regions of underlying vorticity regions smaller than the wavelength [9,10]. Boundary conditions that vary on capillary length scales, as well as wave interactions with structures comparable to or smaller than the wavelength can also lead to wave scattering [11,12], attenuation [13,14], and Bragg reflections [15,16]. Nonetheless, water wave propagation over random underlying currents that vary over *both* large and small length scales, and their interactions, have received relatively less attention.

In this paper, we report results describing the properties of surface wave propagation over both static, and time-varying underlying flows. Rather than computing wave scattering from specific static flow configurations

* Corresponding author. Tel.:+1-310-206-2787.
E-mail address: tomchou@ucla.edu (T. Chou).

PII: S0165-2125(01)00082-8

[9,17,18], we take a statistical approach by considering ensemble averages over realizations of the randomness. Different statistical approaches have been applied to wave propagation over a random depth [19], third sound localization in superfluid Helium films [20], and wave diffusion in the presence of turbulent flows [21–23]. Although random surface flows such as turbulence are in general rotational, we will only consider irrotational underlying flows. Possible applications include uniform flow over a random bottom, generating static random underlying flows, or propagation of a surface wave in a field of randomly generated (e.g. by the wind) surface waves. In the latter case, each surface wave in the field is irrotational, but the underlying flow is time-dependent. We focus on the statistical properties of wave transport over irrotational underlying flows and derive new results with respect to small scale, and time-dependent randomness. Vorticity effects in wave propagation over a spatially gradually varying rotational flow have been considered by White [5]. Although it is straightforward to generalize our statistical approach to include the important effects of vorticity, we will limit our study to Eq. (4) in order to make the development of the transport equations more transparent.

In the next section we derive the linearized capillary–gravity wave equations to lowest order in the irrotational surface flow. The boundary conditions are reduced to two partial differential equations that couple the surface height to velocity potential at the free surface. We treat only the "high frequency" limit [24] where wavelengths are much smaller than the system under consideration. In Section 3, we introduce the Wigner distribution $\boldsymbol{W}(\boldsymbol{x}, \boldsymbol{k}, t)$ [21,24,25] which represents the wave energy density and allows us to treat surface currents that vary simultaneously on two separated length scales. The dynamical equations developed in Section 2 are then written in terms of an evolution equation for $\boldsymbol{W}$. Upon expanding $\boldsymbol{W}$ in powers of (wavelength/propagation distance), we obtain transport equations.

In Section 4, we present our main mathematical result, Eq. (34), an equation describing the transport of surface wave action. Appendix A gives details of some of the derivation. The transport equation includes advection by the slowly varying drift, plus scattering terms that are functions of the correlations of the rapidly varying drift, representing water wave scattering. Upon simultaneously treating both smoothly varying and rapidly varying flows using a two-scale expansion, we find that scattering from the latter depends parametrically on the smoothly varying flows. In Section 5, we discuss the regimes of validity, consider specific forms for the correlation functions, and detail the conditions for Doppler coupling. We find CWA even in the presence of small scale drift variations provided that the correlations of the drift satisfy certain constraints. We also physically motivate the reason for considering two scales for the underlying drift. In the limit of yet larger propagation distances, after multiple wave scattering, wave propagation leaves the transport regime and becomes diffusive when the underlying random flows are static [26].

2. Surface wave equations

Assume an underlying flow $\boldsymbol{V}(\boldsymbol{x}, z, t) \equiv (U_1(\boldsymbol{x}, z, t), U_2(\boldsymbol{x}, z, t), U_z(\boldsymbol{x}, z, t)) \equiv (\boldsymbol{U}(\boldsymbol{x}, z, t), U_z(\boldsymbol{x}, z, t))$, where the 1, 2 components denote the two-dimensional in-plane directions. This flow may be generated by external, time-dependent sources such as wind, internal flows beneath the water surface, as well as other water waves. The surface deformation due to $\boldsymbol{V}(\boldsymbol{x}, z, t)$ is denoted $\bar{\eta}(\boldsymbol{x}, t)$ where $\boldsymbol{x} \equiv (x_1, x_2)$ is the two-dimensional in-plane position vector. An additional variation in height due to the velocity $\boldsymbol{v}(\boldsymbol{x}, z, t)$ associated with a chosen surface wave is denoted $\eta(\boldsymbol{x}, t)$. When all flows are irrotational, we can define their associated velocity potentials $\boldsymbol{V}(\boldsymbol{x}, z, t) \equiv (\nabla_{\boldsymbol{x}} + \hat{\boldsymbol{z}}\partial_z)\Phi(\boldsymbol{x}, z, t)$ and $\boldsymbol{v}(\boldsymbol{x}, z, t) \equiv (\nabla_{\boldsymbol{x}} + \hat{\boldsymbol{z}}\partial_z)\varphi(\boldsymbol{x}, z, t)$. Incompressibility requires

$$\Delta\varphi(\boldsymbol{x}, z, t) + \partial_z^2\varphi(\boldsymbol{x}, z, t) = \Delta\Phi(\boldsymbol{x}, z, t) + \partial_z^2\Phi(\boldsymbol{x}, z, t) = 0, \tag{1}$$

where $\Delta = \nabla_{\boldsymbol{x}}^2$ is the two-dimensional Laplacian. The kinematic condition applied at $z = \bar{\eta}(\boldsymbol{x}, t) + \eta(\boldsymbol{x}, t) \equiv \zeta(\boldsymbol{x}, t)$ is [6]

$$\partial_t\eta(\boldsymbol{x}, t) + \boldsymbol{U}(\boldsymbol{x}, \zeta, t) \cdot \nabla_{\boldsymbol{x}}\zeta(\boldsymbol{x}, t) = U_z(\boldsymbol{x}, z = \zeta, t) + \partial_z\varphi(\boldsymbol{x}, z = \zeta, t). \tag{2}$$

Upon expanding Eq. (2) to linear order in η and φ about the free surface, the right-hand side becomes

$$U_z(\boldsymbol{x},\zeta,t)+\partial_z\varphi(\boldsymbol{x},\zeta,t)=U_z(\boldsymbol{x},\bar{\eta},t)+\eta(\boldsymbol{x},t)\partial_z U_z(\boldsymbol{x},\bar{\eta},t)+\partial_z\boldsymbol{v}(\boldsymbol{x},\bar{\eta},t)+\mathrm{O}(\eta^2). \tag{3}$$

At the surface $z=\bar{\eta}$, $\partial_t\bar{\eta}(x,t)+\boldsymbol{U}(\boldsymbol{x},\bar{\eta},t)\cdot\nabla_{\boldsymbol{x}}\bar{\eta}(\boldsymbol{x},t)=U_z(\boldsymbol{x},\bar{\eta},t)$. Now assume that the underlying flow is weak enough such that $U_z(\boldsymbol{x},z\approx 0,t)$ and $\bar{\eta}$ are both small. A rigid surface approximation is appropriate for small Froude numbers $U^2/c_\phi^2\sim|\nabla_{\boldsymbol{x}}\bar{\eta}|^2\sim U_z(\boldsymbol{x},0,t)/|\boldsymbol{U}(\boldsymbol{x},0,t)|\ll 1$ (c_ϕ is the surface wave phase velocity) and the free surface boundary conditions can be approximately evaluated at $z=0$ [9]. Although we have assumed $U_z(\boldsymbol{x},z\approx 0,t)=\partial_z\Phi(\boldsymbol{x},z\approx 0,t)\approx 0$ and a vanishing surface deformation $\bar{\eta}(\boldsymbol{x},t)\approx 0$, $\nabla_{\boldsymbol{x}}\cdot\boldsymbol{U}(\boldsymbol{x},0,t)=-\partial_z U_z(\boldsymbol{x},0,t)\neq 0$.

Combining the above approximations with the dynamic boundary conditions (derived from balance of normal surface stresses at $z=0$ [6]), we have the pair of coupled equations

$$\begin{aligned}&\partial_t\eta(\boldsymbol{x},t)+\nabla_{\boldsymbol{x}}\cdot(\boldsymbol{U}(\boldsymbol{x},z=0,t)\eta(\boldsymbol{x},t))=\lim_{z\to 0^-}\partial_z\varphi(\boldsymbol{x},z,t),\\&\lim_{z\to 0^-}[\rho\partial_t\varphi(\boldsymbol{x},z,t)+\rho\boldsymbol{U}(\boldsymbol{x},z,t)\cdot\nabla_{\boldsymbol{x}}\varphi(\boldsymbol{x},z,t)]=\sigma\Delta\eta(\boldsymbol{x},t)-\rho g\eta(\boldsymbol{x},t),\end{aligned} \tag{4}$$

where ρ, σ, and g are the water density, air–water surface tension, and gravitational acceleration, respectively. If wavelengths are defined to have scales of O(1), the system size, or distance of wave propagation shown in Fig. 1 is of $\mathrm{O}(L)$ with $L\gg 1$. To implement our high frequency [24] asymptotic analyses, we rescale the system such that all distances are measured in units of $L\equiv\varepsilon^{-1}$. We eventually take the limit $\varepsilon\to 0$ as an approximation for small, finite ε. Surface velocities, potentials, and height displacements are now functions of the new variables $\boldsymbol{x}\to\boldsymbol{x}/\varepsilon$, $z\to z/\varepsilon$ and $t\to t/\varepsilon$. We shall further nondimensionalize all distances in terms of the capillary length $\ell_c=\sqrt{\sigma/g\rho}$. Time, velocity potentials, and velocities are dimensionalized in units of $\sqrt{\ell_c/g}$, $\sqrt{g\ell_c^3}$, and $\sqrt{g\ell_c}$, respectively, e.g. for water, $U=1$ corresponds to a surface drift velocity of ~ 16.3 cm/s.

Since $U_z(\boldsymbol{x},z\approx 0,t)\approx 0$, we define the flow at the surface by

$$\boldsymbol{U}(\boldsymbol{x},z=0,t)\equiv\boldsymbol{U}(\boldsymbol{x},t)+\sqrt{\varepsilon}\delta\boldsymbol{U}\left(\frac{\boldsymbol{x}}{\varepsilon},\frac{t}{\varepsilon}\right). \tag{5}$$

In these rescaled coordinates, $\boldsymbol{U}(\boldsymbol{x},t)$ denotes surface flows varying on length scales of O(1) much greater than a typical wavelength, while $\delta\boldsymbol{U}(\boldsymbol{x}/\varepsilon,t/\varepsilon)$ varies over lengths of $\mathrm{O}(\varepsilon)$ comparable to a typical wavelength. The

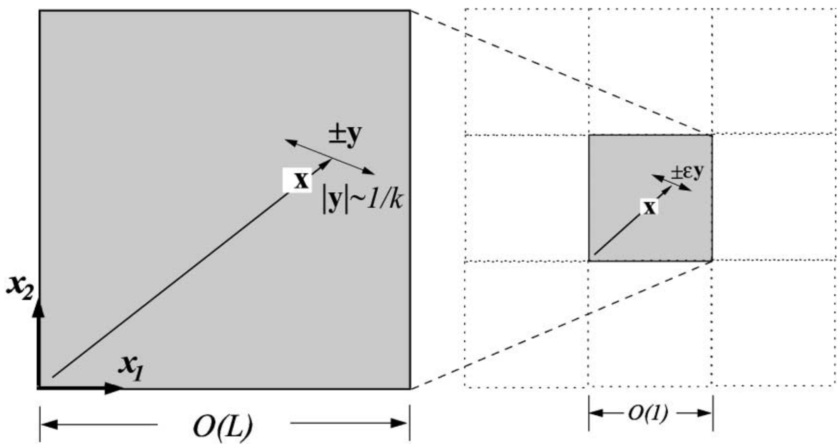

Fig. 1. The relevant scales in water wave transport. Initially, the system size, observation point, and length scale of the slowly varying drift is $\mathrm{O}(L)$, with surface wave wavelength and scale of the random surface current of $\mathrm{O}(1)$. Upon rescaling, the system size becomes $\mathrm{O}(1)$, while the wavelength and random flow variations are $\mathrm{O}(\varepsilon)$.

amplitude of the slowly varying flow $\boldsymbol{U}(\boldsymbol{x},t)$ is $\mathrm{O}(\varepsilon^0)$, while that of the rapidly varying flow $\delta\boldsymbol{U}(\boldsymbol{x}/\varepsilon, t/\varepsilon)$, is assumed to be of $\mathrm{O}(\sqrt{\varepsilon})$. A more detailed discussion of the physical motivation for considering the $\sqrt{\varepsilon}$ scaling is deferred to Section 5. After rescaling, the boundary conditions (4) evaluated at $z=0$ become

$$\begin{aligned}
&\partial_t\eta(\boldsymbol{x},t)+\nabla_{\boldsymbol{x}}\cdot\left[\left(\boldsymbol{U}(\boldsymbol{x},t)+\sqrt{\varepsilon}\delta\boldsymbol{U}\left(\frac{\boldsymbol{x}}{\varepsilon},\frac{t}{\varepsilon}\right)\right)\eta(\boldsymbol{x})\right]=\lim_{z\to0^-}\partial_z\varphi(\boldsymbol{x},0),\\
&\partial_t\varphi(\boldsymbol{x},t)+\boldsymbol{U}(\boldsymbol{x},t)\cdot\nabla_{\boldsymbol{x}}\varphi(\boldsymbol{x},t)+\sqrt{\varepsilon}\delta\boldsymbol{U}\left(\frac{\boldsymbol{x}}{\varepsilon},\frac{t}{\varepsilon}\right)\cdot\nabla_{\boldsymbol{x}}\varphi(\boldsymbol{x},t)=\varepsilon\Delta\eta(\boldsymbol{x},t)-\varepsilon^{-1}\eta(\boldsymbol{x},t).
\end{aligned}\tag{6}$$

In the limiting case where $\delta\boldsymbol{U}=0$ and $\boldsymbol{U}(\boldsymbol{x},t)\equiv\boldsymbol{U}_0$ is strictly uniform, Eq. (11) lead to the familiar capillary–gravity wave dispersion relation

$$\mathsf{H}(\boldsymbol{k})=\sqrt{(k^3+k)\tanh kh}+\boldsymbol{U}_0\cdot\boldsymbol{k}\equiv\Omega(\boldsymbol{k})+\boldsymbol{U}_0\cdot\boldsymbol{k},\tag{7}$$

if all dynamical variables are assumed to follow a time dependence of the form $\mathrm{e}^{-\mathrm{i}\mathsf{H}t}$. Although drift that varies mildly over a wavelength can be treated with characteristics and WKB theory, random flows that varying appreciably over a wavelength require a statistical approach. Without loss of generality, we choose $\delta\boldsymbol{U}$ to have mean zero and an isotropic two-point correlation function $\langle\delta U_i(\boldsymbol{x},t)\delta U_j(\boldsymbol{x}',t')\rangle\equiv R_{ij}(|\boldsymbol{x}-\boldsymbol{x}'|,|t-t'|)$, where $(i,j)=(1,2)$ and $\langle\cdots\rangle$ denotes an ensemble average over realizations of $\delta\boldsymbol{U}(\boldsymbol{x},t)$.

Since $\boldsymbol{x}$ and t play a symmetrical role in the subsequent equations, we introduce the new variable $\boldsymbol{X}=(\boldsymbol{x},t)$ and define the spatial Fourier decompositions for the dynamical wave variables

$$\varphi(\boldsymbol{X},-h\le z\le\zeta)=\int_{\boldsymbol{Q}}\varphi(\boldsymbol{Q})\mathrm{e}^{-\mathrm{i}\boldsymbol{Q}\cdot\boldsymbol{X}}\frac{\cosh q(h+z)}{\cosh qh},\qquad \eta(\boldsymbol{X})=\int_{\boldsymbol{Q}}\eta(\boldsymbol{Q})\mathrm{e}^{-\mathrm{i}\boldsymbol{Q}\cdot\boldsymbol{X}},\tag{8}$$

the surface flows

$$\boldsymbol{U}(\boldsymbol{X})=\int_{\boldsymbol{Q}}\boldsymbol{U}(\boldsymbol{Q})\mathrm{e}^{-\mathrm{i}\boldsymbol{Q}\cdot\boldsymbol{X}},\qquad \delta\boldsymbol{U}\left(\frac{\boldsymbol{X}}{\varepsilon}\right)=\int_{\boldsymbol{Q}}\delta\boldsymbol{U}(\boldsymbol{Q})\mathrm{e}^{-\mathrm{i}\boldsymbol{Q}\cdot\boldsymbol{X}/\varepsilon},\tag{9}$$

and the correlations

$$R_{ij}(\boldsymbol{X})=\int_{\boldsymbol{Q}}R_{ij}(\boldsymbol{Q})\mathrm{e}^{-\mathrm{i}\boldsymbol{Q}\cdot\boldsymbol{X}}.\tag{10}$$

In Eqs. (8) and (9) $\boldsymbol{Q}=(\boldsymbol{q},-\omega_q)=(q_1,q_2,-\omega_q)$, $q\equiv|\boldsymbol{q}|=\sqrt{q_1^2+q_2^2}$, and $\int_{\boldsymbol{Q}}\equiv(2\pi)^{-3}\int\mathrm{d}q_1\,\mathrm{d}q_2\int_{-\infty}^{+\infty}\mathrm{d}\omega_q$. We similarly define $\boldsymbol{P}\equiv(\boldsymbol{p},-\omega_p)$ and $\boldsymbol{K}\equiv(\boldsymbol{k},-\omega_k)$ for subsequent analyses. The Fourier integrals for η exclude $\boldsymbol{q}=0$ due to the incompressibility constraint $\int_{\boldsymbol{x}}\eta(\boldsymbol{x},t)=0$, while the $\boldsymbol{q}=0$ mode for φ gives an irrelevant constant shift to the velocity potential. Note that φ in Eq. (8) manifestly satisfies Laplace's Eq. (9). Substituting Eq. (9) into the boundary conditions, we obtain,

$$\begin{aligned}
&\mathrm{i}\omega_k\eta(\boldsymbol{K})-\mathrm{i}\int_{\boldsymbol{Q}}\eta(\boldsymbol{K}-\boldsymbol{Q})\boldsymbol{U}(\boldsymbol{Q})\cdot\boldsymbol{k}-\mathrm{i}\sqrt{\varepsilon}\int_{\boldsymbol{Q}}\eta\left(\frac{\boldsymbol{K}-\boldsymbol{Q}}{\varepsilon}\right)\delta\boldsymbol{U}(\boldsymbol{Q})\cdot\boldsymbol{k}=\varphi(\boldsymbol{K})\,k\tanh\varepsilon kh,\\
&\mathrm{i}\omega_k\varphi(\boldsymbol{K})-\mathrm{i}\int_{\boldsymbol{Q}}\boldsymbol{U}(\boldsymbol{Q})\cdot(\boldsymbol{k}-\boldsymbol{q})\varphi(\boldsymbol{K}-\boldsymbol{Q})-\mathrm{i}\sqrt{\varepsilon}\int_{\boldsymbol{Q}}\delta\boldsymbol{U}(\boldsymbol{Q})\cdot\left(\frac{\boldsymbol{K}-\boldsymbol{Q}}{\varepsilon}\right)\varphi\left(\frac{\boldsymbol{K}-\boldsymbol{Q}}{\varepsilon}\right)\\
&\quad=-(\varepsilon k^2+\varepsilon^{-1})\eta(\boldsymbol{K}),
\end{aligned}\tag{11}$$

where the $\delta\boldsymbol{U}(\boldsymbol{Q})$ are correlated according to

$$\langle\delta U_i(\boldsymbol{P})\delta U_j(\boldsymbol{Q})\rangle=R_{ij}(|\boldsymbol{P}|)\delta(\boldsymbol{P}+\boldsymbol{Q}).\tag{12}$$

Since the correlation $R_{ij}(\boldsymbol{X})$ is symmetric in $i\leftrightarrow j$, and depends only upon the magnitude $|\boldsymbol{X}|$, $R_{ij}(|\boldsymbol{P}-\boldsymbol{Q}|)$ is real. Here, $(|\boldsymbol{P}-\boldsymbol{Q}|)$ represents $(|\boldsymbol{p}-\boldsymbol{q}|,|\omega_p-\omega_q|)$.

3. The Wigner distribution and asymptotic analyses

The intensity of the dynamical wave variables can be represented by the product of two Green functions evaluated at points $\boldsymbol{X} \pm \varepsilon \boldsymbol{Y}/2$, where $\boldsymbol{Y} \equiv (\boldsymbol{y}, t)$. The difference in their evaluation points, $\varepsilon \boldsymbol{Y}$, resolves the waves of wave vector $|\boldsymbol{k}| \sim 2\pi/(\varepsilon y)$ and frequency $\omega \sim 2\pi/(\varepsilon t)$. Elter and Molyneux [19] used this representation to study shallow water wave propagation over a random bottom. However, for the finite depth surface wave problem, where the Green function is not simple, and where two length scales are treated, it is convenient to use the Fourier representation of the Wigner distribution [24,27,28].

Define $\boldsymbol{\psi} = (\psi_1, \psi_2) \equiv (\eta(\boldsymbol{X}), \varphi(\boldsymbol{X}, z = 0))$ and the Wigner distribution:

$$W_{ij}(\boldsymbol{X}, \boldsymbol{K}) \equiv (2\pi)^{-3} \int \mathrm{e}^{\mathrm{i}\boldsymbol{K}\cdot\boldsymbol{Y}} \psi_i \left(\boldsymbol{X} - \frac{\varepsilon \boldsymbol{Y}}{2}\right) \psi_j^* \left(\boldsymbol{X} + \frac{\varepsilon \boldsymbol{Y}}{2}\right) \mathrm{d}\boldsymbol{Y}, \tag{13}$$

where $\boldsymbol{X}$ is a central field point from which we consider two neighboring points $\boldsymbol{X} \pm \varepsilon \boldsymbol{Y}/2$, and their intervening wave field. Fourier transforming the $\boldsymbol{X}$ variable using Eq. (8) we find,

$$W_{ij}(\boldsymbol{P}, \boldsymbol{K}) = (2\pi\varepsilon)^{-3} \psi_i \left(\frac{\boldsymbol{P}}{2} - \frac{\boldsymbol{K}}{\varepsilon}\right) \psi_j^* \left(-\frac{\boldsymbol{P}}{2} - \frac{\boldsymbol{K}}{\varepsilon}\right). \tag{14}$$

The total wave energy, comprising gravitational, kinetic, and surface tension contributions is

$$\begin{aligned} E &= \frac{1}{2}\int_{\boldsymbol{x}} \left[|\nabla_{\boldsymbol{x}}\eta|^2 + |\eta|^2\right] + \frac{1}{2}\int_{\boldsymbol{x}}\int_{-h}^{0} \mathrm{d}z\, |\boldsymbol{U} + \hat{\boldsymbol{z}}U_z + \boldsymbol{v}|^2 - \frac{1}{2}\int_{\boldsymbol{x}}\int_{-h}^{0} \mathrm{d}z\, |\boldsymbol{U} + \hat{\boldsymbol{z}}U_z|^2 \\ &= \frac{1}{2}\int_{\boldsymbol{k}} (k^2+1)|\eta(\boldsymbol{k})|^2 + k \tanh kh\, |\varphi(\boldsymbol{k}, z=0)|^2. \end{aligned} \tag{15}$$

The energy above has been expanded to an order in $\eta(\boldsymbol{x}, t)$ and $\varphi(\boldsymbol{x}, z, t)$ consistent with the approximations used to derive Eq. (4). In arriving at the last equality in (15), we have integrated by parts, used the Fourier decompositions and imposed an impenetrable bottom condition at $z = -h$. The wave energy density carried by wave vector $\boldsymbol{k}$ and frequency ω_k is [28]

$$E(\boldsymbol{X}, \boldsymbol{K}) = \tfrac{1}{2}\mathrm{Tr}[\boldsymbol{A}(\boldsymbol{k})\boldsymbol{W}(\boldsymbol{X}, \boldsymbol{K})], \tag{16}$$

where $A_{11}(\boldsymbol{k}) = k^2 + 1$, $A_{22}(\boldsymbol{k}) = k \tanh kh$, $A_{12} = A_{21} = 0$.

In the presence of slowly varying drift, we identify $\boldsymbol{W}(\boldsymbol{X}, \boldsymbol{K})$ as the *local* Wigner distribution at position $\boldsymbol{x}$ and time t representing waves of wave vector $\boldsymbol{k}$ with fast frequency ω_k. An equation for its Fourier transform $\boldsymbol{W}(\boldsymbol{P}, \boldsymbol{K})$ can be derived by considering the equation for the vector field $\boldsymbol{\psi}$ implied by the boundary conditions (Eq. (4)):

$$\mathrm{i}L_{j\ell}(\boldsymbol{K})\psi_\ell(\boldsymbol{K}) = \mathrm{i}\int_{\boldsymbol{Q}} \boldsymbol{U}(\boldsymbol{Q}) \cdot (\boldsymbol{k} - \boldsymbol{q}\delta_{j2})\psi_j(\boldsymbol{K} - \boldsymbol{Q}) + \mathrm{i}\sqrt{\varepsilon}\int_{\boldsymbol{Q}} \delta\boldsymbol{U}(\boldsymbol{Q}) \cdot \left(\boldsymbol{k} - \frac{\boldsymbol{q}}{\varepsilon}\delta_{j2}\right)\psi_j\left(\boldsymbol{K} - \frac{\boldsymbol{Q}}{\varepsilon}\right), \tag{17}$$

where the operator $\boldsymbol{L}(\boldsymbol{K})$ is defined by

$$\boldsymbol{L}(\boldsymbol{K}) = \begin{pmatrix} \omega_k & \mathrm{i}|\boldsymbol{k}| \tanh \varepsilon|\boldsymbol{k}|h \\ -\mathrm{i}(\varepsilon k^2 + \varepsilon^{-1}) & \omega_k \end{pmatrix}. \tag{18}$$

We have redefined the physical wave number to be k/ε so that $k \sim \mathrm{O}(1)$. Upon using Eqs. (14) and (17), (see Appendix A)

$$\begin{aligned} \mathrm{i}L_{j\ell}\left(\frac{\boldsymbol{P}}{2} - \frac{\boldsymbol{K}}{\varepsilon}\right) W_{ij}(\boldsymbol{P}, \boldsymbol{K}) = {} & \mathrm{i}\int_{\boldsymbol{Q}} \boldsymbol{U}(\boldsymbol{Q}) \cdot \left(-\frac{\boldsymbol{k}}{\varepsilon} + \frac{\boldsymbol{p}}{2} - \boldsymbol{q}\delta_{j2}\right) W_{ij}\left(\boldsymbol{P} - \boldsymbol{Q}, \boldsymbol{K} + \frac{\varepsilon\boldsymbol{Q}}{2}\right) \\ & + \mathrm{i}\sqrt{\epsilon}\int_{\boldsymbol{Q}} \delta\boldsymbol{U}(\boldsymbol{Q}) \cdot \left(-\frac{\boldsymbol{k}}{\varepsilon} + \frac{\boldsymbol{p}}{2} - \frac{\boldsymbol{q}}{\varepsilon}\delta_{j2}\right) W_{ij}\left(\boldsymbol{P} - \frac{\boldsymbol{Q}}{\varepsilon}, \boldsymbol{K} + \frac{\boldsymbol{Q}}{2}\right). \end{aligned} \tag{19}$$

If we now assume that $\boldsymbol{W}(\boldsymbol{P},\boldsymbol{K})$ can be represented by functions that vary independently at the two relevant length and time scales, $\boldsymbol{P} \to \boldsymbol{P} + \boldsymbol{\Xi}/\varepsilon$ (where $\boldsymbol{\Xi} \equiv (\boldsymbol{\xi}, -\omega_\xi)$). This amounts to the Fourier equivalent of a two-scale expansion where $\boldsymbol{X}$ is replaced by $\boldsymbol{X}$ and $\boldsymbol{Y} = \boldsymbol{X}/\varepsilon$ [24]. The two new independent wave vectors $\boldsymbol{P}$ and $\boldsymbol{\Xi}$ are both of O(1). Expanding the Wigner distribution in powers of $\sqrt{\varepsilon}$,

$$\boldsymbol{W}(\boldsymbol{P},\boldsymbol{K}) \to \boldsymbol{W}_0(\boldsymbol{P},\boldsymbol{\Xi},\boldsymbol{K}) + \sqrt{\varepsilon}\boldsymbol{W}_{1/2}(\boldsymbol{P},\boldsymbol{\Xi},\boldsymbol{K}) + \varepsilon \boldsymbol{W}_1(\boldsymbol{P},\boldsymbol{\Xi},\boldsymbol{K}) + \mathrm{O}(\varepsilon^{3/2}). \tag{20}$$

We expand each quantity appearing in Eq. (19) in powers of $\sqrt{\varepsilon}$ and equate like powers. Expanding $\boldsymbol{L}(-\boldsymbol{K}/\varepsilon+\boldsymbol{P}/2) = \varepsilon^{-1}\boldsymbol{L}_0(\boldsymbol{K}) + \boldsymbol{L}_1(\boldsymbol{K},\boldsymbol{P}) + \mathrm{O}(\varepsilon)$, we have

$$\boldsymbol{L}_0(\boldsymbol{K}) = \begin{pmatrix} -\omega_k & \mathrm{i}k\tanh kh \\ -\mathrm{i}(k^2+1) & -\omega_k \end{pmatrix}, \qquad \boldsymbol{L}_1(\boldsymbol{K},\boldsymbol{P}) \equiv \begin{pmatrix} \frac{1}{2}\omega_p & \mathrm{i}\boldsymbol{p}\cdot\boldsymbol{k} f(k) \\ \mathrm{i}\boldsymbol{p}\cdot\boldsymbol{k} & \frac{1}{2}\omega_p \end{pmatrix}, \tag{21}$$

where

$$f(k) \equiv -\frac{hk + \sinh kh \cosh kh}{2k\cosh^2 kh}. \tag{22}$$

3.1. Order ε^{-1} terms

Upon subtracting its adjoint from Eq. (19), and collecting terms of $\mathrm{O}(\varepsilon^{-1})$,

$$\boldsymbol{W}_0(\boldsymbol{P},\boldsymbol{\Xi},\boldsymbol{K})\boldsymbol{L}_0^\dagger(\boldsymbol{K}_+) - \boldsymbol{L}_0(\boldsymbol{K}_-)\boldsymbol{W}_0(\boldsymbol{P},\boldsymbol{\Xi},\boldsymbol{K}) = 0, \tag{23}$$

where $\boldsymbol{K}_\pm \equiv \boldsymbol{K} \pm \boldsymbol{\Xi}/2$. To solve Eq. (23), we use the eigenvalues and normalized eigenvectors for $\boldsymbol{L}_0$ and its complex adjoint $\boldsymbol{L}_0^\dagger$. The eigenvectors corresponding to the eigenvalues $\tau\Omega(\boldsymbol{k}) - \omega_k - \mathrm{i}\gamma$ and $\tau\Omega(\boldsymbol{k}) - \omega_k + \mathrm{i}\gamma$ are

$$\boldsymbol{b}_\tau = \begin{pmatrix} \mathrm{i}\tau\sqrt{\dfrac{\alpha(\boldsymbol{k})}{2}} \\ \dfrac{1}{\sqrt{2\alpha(\boldsymbol{k})}} \end{pmatrix} \quad \text{and} \quad \boldsymbol{c}_\tau = \begin{pmatrix} \dfrac{\mathrm{i}\tau}{\sqrt{2\alpha(\boldsymbol{k})}} \\ \dfrac{\sqrt{\alpha(\boldsymbol{k})}}{2} \end{pmatrix}, \tag{24}$$

respectively, where $\alpha(\boldsymbol{k}) \equiv \Omega(\boldsymbol{k})/k^2 + 1$, and $\tau = \pm 1$. The physical origin of the small imaginary term $\mathrm{i}\gamma$ arises from causality, but can also be explicitly derived from considerations of an infinitesimally small viscous dissipation [11]. Although we have assumed $\gamma \to 0$, for our model to be valid, the viscosity need only be small enough such that surface waves are not attenuated before they have a chance to multiply scatter and enter the transport or diffusion regimes. Since in the frequency domain, wave dissipation is given by $\gamma = 2\nu k^2$ [29] where ν is the kinematic viscosity and $c_\mathrm{g}(k) \equiv |\nabla_{\boldsymbol{k}}\Omega(k)|$ is the group velocity, the corresponding decay length $k_\mathrm{d}^{-1} \sim c_\mathrm{g}(k)/(\nu k^2)$ must be greater than the relevant wave propagation distance. Therefore,

$$\varepsilon^2 c_\mathrm{g}(k) \gg 2\pi\nu k^2, \tag{25}$$

for transport to survive dissipation. The inequality (25) is most easily satisfied in the shallow water wave regime for transport. Even in deep water, for 100 cm waves, criterion (25) requires $\varepsilon \gg 6 \times 10^{-4}$, providing an ample regime for transport behavior to take hold. For 10 cm waves, the criterion is $\varepsilon \gg 2 \times 10^{-3}$.

A solution that manifestly satisfies Eq. (23) is constructed by expanding in the basis of 2×2 matrices composed from the eigenvectors

$$\boldsymbol{W}_0(\boldsymbol{P},\boldsymbol{\Xi},\boldsymbol{K}) = \delta(\boldsymbol{\Xi}) \sum_{\tau,\tau'=\pm} a_{\tau\tau'}(\boldsymbol{P},\boldsymbol{K})\boldsymbol{b}_\tau(\boldsymbol{k}_-)\boldsymbol{b}_{\tau'}^\dagger(\boldsymbol{k}_+), \tag{26}$$

where the $\delta(\boldsymbol{\Xi})$ constraint arises from imposing the condition that $\boldsymbol{L}_0$ in Eq. (26) defines the high frequency dispersion relation. Upon right[left] multiplying Eq. (26) by the eigenvectors of the adjoint problem, $\boldsymbol{c}_\tau(\boldsymbol{k}_-)[\boldsymbol{c}_\tau^\dagger(\boldsymbol{k}_+)]$, we find $a_{+-} = a_{-+} = 0$, and $a_{--}(\boldsymbol{P}, \boldsymbol{\Xi}, \boldsymbol{K}) \equiv a_-(\boldsymbol{P}, \boldsymbol{\Xi}, \boldsymbol{K}) = a_{++}(\boldsymbol{P}, \boldsymbol{\Xi}, -\boldsymbol{K}) \equiv a_+(\boldsymbol{P}, \boldsymbol{\Xi}, -\boldsymbol{K}) \neq 0$ only if $\boldsymbol{\Xi} = 0$. From the leading order in Eq. (19) we deduce

$$a_\tau(\boldsymbol{X}, \boldsymbol{K}) = a_\tau(\boldsymbol{X}, \boldsymbol{k})\delta(\omega_k + \tau \mathsf{H}(\boldsymbol{X}, \boldsymbol{k})), \tag{27}$$

where

$$\mathsf{H}(\boldsymbol{X}, \boldsymbol{k}) = \mathsf{H}(\boldsymbol{x}, \boldsymbol{k}, t) = \sqrt{(k^3 + k)\tanh kh} + \boldsymbol{U}_0(\boldsymbol{x}, t) \cdot \boldsymbol{k}. \tag{28}$$

This relation states that high frequencies ω_k are related to wave number through the familiar capillary–gravity wave dispersion relation.

From the definition of $\boldsymbol{W}_0$, we see that the $(1, 1)$ component of $\boldsymbol{W}_0$ is the local envelop of the ensemble averaged wave intensity $|\eta(\boldsymbol{X}, \boldsymbol{K})|^2 \simeq a_+(\boldsymbol{X}, \boldsymbol{K})\alpha(\boldsymbol{k})$. Similarly, from the energy (Eq. (16)), we see immediately that the local ensemble averaged energy density

$$\langle E(\boldsymbol{X}, \boldsymbol{K})\rangle = A_{11}(\boldsymbol{k})\alpha(\boldsymbol{k})\langle a(\boldsymbol{X}, \boldsymbol{K})\rangle + A_{22}(\boldsymbol{k})\langle a(\boldsymbol{X}, \boldsymbol{K})\rangle = \Omega(\boldsymbol{k})\langle a(\boldsymbol{X}, \boldsymbol{K})\rangle, \tag{29}$$

where $a(\boldsymbol{X}, \boldsymbol{K}) = a_+(\boldsymbol{X}, \boldsymbol{K})$. Therefore, since the starting dynamical equations are linear, we can identify $\langle a(\boldsymbol{X}, \boldsymbol{K})\rangle$ as the ensemble averaged local wave action associated with waves of wave vector $\boldsymbol{k}$ [30] and frequency ω_k determined by the usual dispersion relation (Eqs. (27) and (28)). The wave action $\langle a(\boldsymbol{X}, \boldsymbol{K})\rangle$, rather than the energy density $\langle E(\boldsymbol{X}, \boldsymbol{K})\rangle$ is the conserved quantity [3,4,6].

3.2. Order $\varepsilon^{-1/2}$ terms

Collecting terms of order $\varepsilon^{-1/2}$ in the symmetrised form of Eq. (19), we obtain

$$\begin{aligned}
&\boldsymbol{W}_{1/2}(\boldsymbol{P}, \boldsymbol{\Xi}, \boldsymbol{K})\boldsymbol{L}_0^\dagger(\boldsymbol{K}_+) - \boldsymbol{L}_0(\boldsymbol{K}_-)\boldsymbol{W}_{1/2}(\boldsymbol{P}, \boldsymbol{\Xi}, \boldsymbol{K}) + \int_{\boldsymbol{Q}} \boldsymbol{U}(\boldsymbol{Q}) \cdot \boldsymbol{\xi}\, \boldsymbol{W}_{1/2}(\boldsymbol{P} \\
&-\boldsymbol{Q}, \boldsymbol{\Xi} - \boldsymbol{Q}, \boldsymbol{K}) - \int_{\boldsymbol{Q}} \delta\boldsymbol{U}(\boldsymbol{Q}) \cdot \boldsymbol{k}_-\, \boldsymbol{W}_0\left(\frac{\boldsymbol{P}, \boldsymbol{\Xi} - \boldsymbol{Q}, \boldsymbol{K} + \boldsymbol{Q}}{2}\right) + \int_{\boldsymbol{Q}} \delta\boldsymbol{U}(\boldsymbol{Q}) \cdot \boldsymbol{k}_+ \boldsymbol{W}_0\left(\frac{\boldsymbol{P}, \boldsymbol{\Xi} - \boldsymbol{Q}, \boldsymbol{K} - \boldsymbol{Q}}{2}\right) \\
&-\int_{\boldsymbol{Q}} \delta\boldsymbol{U}(\boldsymbol{Q}) \cdot \boldsymbol{q}\left[\boldsymbol{W}_0\left(\frac{\boldsymbol{P}, \boldsymbol{\Xi} - \boldsymbol{Q}, \boldsymbol{K} + \boldsymbol{Q}}{2}\right)\boldsymbol{S} + \boldsymbol{S}\,\boldsymbol{W}_0\left(\frac{\boldsymbol{P}, \boldsymbol{\Xi} - \boldsymbol{Q}, \boldsymbol{K} - \boldsymbol{Q}}{2}\right)\right] = 0,
\end{aligned} \tag{30}$$

where

$$\boldsymbol{S} = \begin{bmatrix} 0 & 0 \\ 0 & 1 \end{bmatrix}.$$

Similarly, decomposing $\boldsymbol{W}_{1/2}$ in the basis matrices composed of $\boldsymbol{b}_\tau(\boldsymbol{k}_-)\boldsymbol{b}_{\tau'}^\dagger(\boldsymbol{k}_+)$ (as in Eq. (26)), substituting $\boldsymbol{W}_0(\boldsymbol{P}, \boldsymbol{K})\delta(\boldsymbol{\Xi})$ from Eq. (26) into the above, and inverse Fourier transforming in the slow variable $\boldsymbol{P}$, we obtain

$$\boldsymbol{W}_{1/2}(\boldsymbol{X}, \boldsymbol{\Xi}, \boldsymbol{K}) = \sum_{\tau,\tau'=\pm} \frac{\delta\boldsymbol{U}(\boldsymbol{\Xi}) \cdot \boldsymbol{\Gamma}_{\tau,\tau'}(\boldsymbol{X}, \boldsymbol{\xi}, \boldsymbol{K})\boldsymbol{b}_\tau(\boldsymbol{k}_-)\boldsymbol{b}_{\tau'}^\dagger(\boldsymbol{k}_+)\delta(\omega_k + \tau \mathsf{H})}{\omega_{k_-} - \omega_{k_+} + \tau'\Omega(\boldsymbol{k}_+) - \tau\Omega(\boldsymbol{k}_-) + \boldsymbol{U}(\boldsymbol{X}) \cdot \boldsymbol{\xi} + 2\mathrm{i}\gamma}, \tag{31}$$

where

$$\begin{aligned}
\boldsymbol{\Gamma}_{\tau,\tau'}(\boldsymbol{X}, \boldsymbol{\xi}, \boldsymbol{K}) \equiv{}& \boldsymbol{k}_- a_{\tau'}(\boldsymbol{X}, \boldsymbol{K}_+)\boldsymbol{c}_\tau^\dagger(\boldsymbol{k}_-)\boldsymbol{b}_{\tau'}(\boldsymbol{k}_+) - \boldsymbol{k}_+ a_\tau(\boldsymbol{X}, \boldsymbol{K}_-)\boldsymbol{b}_\tau^\dagger(\boldsymbol{k}_-)\boldsymbol{c}_{\tau'}(\boldsymbol{k}_+) \\
&+ \frac{\boldsymbol{\xi}}{2}\sum_{\mu=\pm}[a_\mu(\boldsymbol{X}, \boldsymbol{K}_+)\boldsymbol{c}_\tau^\dagger(\boldsymbol{k}_-)\boldsymbol{b}_\mu(\boldsymbol{k}_+) + a_\mu(\boldsymbol{X}, \boldsymbol{K}_-)\boldsymbol{b}_\mu^\dagger(\boldsymbol{k}_-)\boldsymbol{c}_{\tau'}(\boldsymbol{k}_+)].
\end{aligned} \tag{32}$$

3.3. Order ε^0 terms

The terms of order ε^0 contained in the symmetrised form of Eq. (19) read

$$
\begin{aligned}
&\mathrm{i}\boldsymbol{W}_0(\boldsymbol{P},\boldsymbol{K})\boldsymbol{L}_1^\dagger(-\boldsymbol{P}) - \mathrm{i}\boldsymbol{L}_1(\boldsymbol{P})\boldsymbol{W}_0(\boldsymbol{P},\boldsymbol{K}) - \mathrm{i}\int_{\boldsymbol{Q}} \boldsymbol{k}\cdot\boldsymbol{U}(\boldsymbol{Q})\boldsymbol{q}\cdot\nabla_{\boldsymbol{k}}\boldsymbol{W}_0(\boldsymbol{P}-\boldsymbol{Q},\boldsymbol{\Xi},\boldsymbol{K})\\
&\quad+\mathrm{i}\int_{\boldsymbol{Q}} \boldsymbol{U}(\boldsymbol{Q})\cdot\boldsymbol{p}\,\boldsymbol{W}_0(\boldsymbol{P}-\boldsymbol{Q},\boldsymbol{\Xi},\boldsymbol{K}) + \mathrm{i}\int_{\boldsymbol{Q}} \delta\boldsymbol{U}(\boldsymbol{Q})\cdot\boldsymbol{k}_+\,\boldsymbol{W}_{1/2}\left(\boldsymbol{P},\boldsymbol{\Xi}-\boldsymbol{Q},\boldsymbol{K}-\frac{\boldsymbol{Q}}{2}\right)\\
&\quad-\mathrm{i}\int_{\boldsymbol{Q}} \boldsymbol{U}(\boldsymbol{Q})\cdot\boldsymbol{q}[\boldsymbol{S}\,\boldsymbol{W}_0(\boldsymbol{P}-\boldsymbol{Q},\boldsymbol{\Xi},\boldsymbol{K}) + \boldsymbol{W}_0(\boldsymbol{P}-\boldsymbol{Q},\boldsymbol{\Xi},\boldsymbol{K})\boldsymbol{S}]\\
&\quad-\mathrm{i}\int_{\boldsymbol{Q}} \delta\boldsymbol{U}(\boldsymbol{Q})\cdot\boldsymbol{k}_-\,\boldsymbol{W}_{1/2}\left(\boldsymbol{P},\boldsymbol{\Xi}-\boldsymbol{Q},\boldsymbol{K}+\frac{\boldsymbol{Q}}{2}\right)\\
&\quad-\int_{\boldsymbol{Q}} \delta\boldsymbol{U}(\boldsymbol{Q})\cdot\boldsymbol{q}\left[\boldsymbol{S}\,\boldsymbol{W}_{1/2}\left(\boldsymbol{P},\boldsymbol{\Xi}-\boldsymbol{Q},\boldsymbol{K}+\frac{\boldsymbol{Q}}{2}\right) + \boldsymbol{W}_{1/2}\left(\boldsymbol{P},\boldsymbol{\Xi}-\boldsymbol{Q},\boldsymbol{K}-\frac{\boldsymbol{Q}}{2}\right)\boldsymbol{S}\right]\\
&\quad+\mathrm{i}\boldsymbol{W}_1\boldsymbol{L}_0^\dagger - \mathrm{i}\boldsymbol{L}_0\boldsymbol{W}_1 + \int_{\boldsymbol{Q}} \boldsymbol{U}(\boldsymbol{Q})\cdot\boldsymbol{\xi}\boldsymbol{W}_1(\boldsymbol{P}-\boldsymbol{Q},\boldsymbol{\Xi},\boldsymbol{K}) = 0.
\end{aligned}
\tag{33}
$$

To obtain an equation for the statistical ensemble average $\langle a_+(\boldsymbol{X},\boldsymbol{K})\rangle$, we left-multiply Eq. (33) by $\boldsymbol{c}_+^\dagger(\boldsymbol{k})$ and right-multiply by $\boldsymbol{c}_+(\boldsymbol{k})$ and substitute $\boldsymbol{W}_{1/2}$ from Eq. (31). We obtain a closed equation for $a(\boldsymbol{X},\boldsymbol{K}) \equiv \langle a_+(\boldsymbol{X},\boldsymbol{K})\rangle$ (we henceforth suppress the $\langle\cdots\rangle$ notation for $a(\boldsymbol{X},\boldsymbol{K})$ and $E(\boldsymbol{X},\boldsymbol{K})$) by truncating terms containing $\boldsymbol{W}_1$. Clearly, from Eq. (24), $\boldsymbol{c}_+^\dagger(\boldsymbol{k})(\mathrm{i}\boldsymbol{W}_1\boldsymbol{L}_0^\dagger - \mathrm{i}\boldsymbol{L}_0\boldsymbol{W}_1)\boldsymbol{c}_+(\boldsymbol{k}) = 0$. Furthermore, we assume $\langle\boldsymbol{\xi}\,\boldsymbol{W}_1(\boldsymbol{P}-\boldsymbol{Q},\boldsymbol{\Xi},\boldsymbol{K})\rangle \approx 0$ which follows from ergodicity of dynamical systems, and has been used in the propagation of waves in random media (see [24,31]). The transport equations resulting from this truncation are rigorously justified in the scalar case [32,33].

4. The surface wave transport equation

The main mathematical result of this paper, an evolution equation for the ensemble averaged wave action $a(\boldsymbol{x},\boldsymbol{k},t)$ (recall that $a_+(\boldsymbol{X},\boldsymbol{K}) = a(\boldsymbol{x},\boldsymbol{k},t)\delta(\omega_k \pm \mathsf{H}(\boldsymbol{x},\boldsymbol{k},t))$) follows from Eq. (33) above (cf. Appendix A) and reads,

$$
\begin{aligned}
&\partial_t a(\boldsymbol{x},\boldsymbol{k},t) + \nabla_{\boldsymbol{k}}\mathsf{H}(\boldsymbol{x},\boldsymbol{k},t)\cdot\nabla_{\boldsymbol{x}}a(\boldsymbol{x},\boldsymbol{k},t) - \nabla_{\boldsymbol{x}}\mathsf{H}(\boldsymbol{x},\boldsymbol{k},t)\cdot\nabla_{\boldsymbol{k}}a(\boldsymbol{x},\boldsymbol{k},t)\\
&= -\Sigma(\boldsymbol{x},\boldsymbol{k},t)a(\boldsymbol{x},\boldsymbol{k},t) + \int_{\boldsymbol{Q}} \sigma(\boldsymbol{q},\boldsymbol{k},\boldsymbol{x},t)a(\boldsymbol{x},\boldsymbol{q},t),
\end{aligned}
\tag{34}
$$

where H is given in Eq. (28). The left-hand side in Eq. (34) corresponds to wave action propagation in the absence of random fluctuations. It is equivalent to the equations obtained by the ray theory, or a WKB expansion (see Section 5.1). The two terms on the right-hand side of Eq. (34) represent refraction, or “scattering” of wave action out of and into waves with wave vector $\boldsymbol{k}$, respectively. In deriving Eq. (34) we have inverse Fourier transformed back to the slow field point variable $\boldsymbol{x}$, and used the relation $(\alpha(\boldsymbol{k}) - f(k)\alpha^{-1}(\boldsymbol{k}))\boldsymbol{k} \equiv \nabla_{\boldsymbol{k}}\Omega(\boldsymbol{k})$. We also assumed $R_{ij}(\boldsymbol{Q})q_i = R_{ij}(\boldsymbol{Q})q_j = 0$, which would always be valid for divergence-free flows in two dimensions. Although the perturbation $\delta\boldsymbol{U}$ is not divergence-free in general, $\nabla\cdot\delta\boldsymbol{U}(\boldsymbol{X},z=0) = -\partial_z\delta U_z(\boldsymbol{X},0) \neq 0$, by using symmetry considerations, we will show in Section 5.2 that $R_{ij}(\boldsymbol{Q})q_i = R_{ij}(\boldsymbol{Q})q_j = 0$.

The scattering rates are

$$\Sigma(\boldsymbol{x},\boldsymbol{k},t) \equiv 2\pi \sum_{\tau=\pm} \int \mathrm{d}\boldsymbol{q}\,\mathrm{d}\omega\, q_i R_{ij}(\boldsymbol{q}-\boldsymbol{k},\omega)k_j \boldsymbol{b}_+^\dagger(\boldsymbol{k})\boldsymbol{c}_\tau(\boldsymbol{q})\boldsymbol{b}_\tau^\dagger(\boldsymbol{q})\boldsymbol{c}_+(\boldsymbol{k}) \times \delta(\omega-\tau \mathsf{H}(\boldsymbol{x},\tau\boldsymbol{q},t)+\mathsf{H}(\boldsymbol{x},\boldsymbol{k},t)),$$

$$\sigma(\boldsymbol{x},\boldsymbol{q},\boldsymbol{k},t) \equiv 2\pi \sum_{\tau=\pm} \int \mathrm{d}\boldsymbol{q}\,\mathrm{d}\omega\, \tau q_i R_{ij}(\tau\boldsymbol{q}-\boldsymbol{k},\omega)k_j |\boldsymbol{b}_\tau^\dagger(\tau\boldsymbol{q})\boldsymbol{c}_+(\boldsymbol{k})|^2 \times\delta(\omega-\tau \mathsf{H}(\boldsymbol{x},\boldsymbol{q},t)+\mathsf{H}(\boldsymbol{x},\boldsymbol{k},t)), \tag{35}$$

where

$$\boldsymbol{b}_+^\dagger(\boldsymbol{k})\boldsymbol{c}_\tau(\boldsymbol{q})\boldsymbol{b}_\tau^\dagger(\boldsymbol{q})\boldsymbol{c}_+(\boldsymbol{k}) = \frac{(\tau\alpha(\boldsymbol{k})+\alpha(\boldsymbol{q}))(\tau\alpha(\boldsymbol{q})+\alpha(\boldsymbol{k}))}{4\alpha(\boldsymbol{k})\alpha(\boldsymbol{q})}, \qquad |\boldsymbol{b}_\tau^\dagger(\boldsymbol{k})\boldsymbol{c}_{\tau'}(\boldsymbol{q})|^2 = \frac{(\tau\alpha(\boldsymbol{q})+\alpha(\boldsymbol{k}))^2}{4\alpha(\boldsymbol{k})\alpha(\boldsymbol{q})}. \tag{36}$$

Physically, $\Sigma(\boldsymbol{x},\boldsymbol{k},t)$ is a decay rate arising from scattering of action out of wave vector $\boldsymbol{k}$. The typical distance traveled by a wave before it is significantly redirected, or converted into different frequency modes, is defined by the mean free path

$$\ell_{\mathrm{mfp}} = \frac{c_{\mathrm{g}}(k)}{\Sigma(k)} \sim \mathrm{O}(1). \tag{37}$$

The mean free path described here carries a different interpretation from that considered in weakly nonlinear, or multiple scattering theories [25,34] where one treats a low density of scatterers. Rather than strong, rare scatterings over every distance $\ell_{\mathrm{mfp}} \sim \mathrm{O}(1)$, we have considered constant, but weak interaction with an extended, random flow field. Although here, each scattering is $\mathrm{O}(\varepsilon)$ and weak, over a distance of O(1), approximately ε^{-1} interactions arise, ultimately producing $\ell_{\mathrm{mfp}} \sim \mathrm{O}(1)$. The kernel $\sigma(\boldsymbol{x},\boldsymbol{q},\boldsymbol{k},t)$ represents scattering of action from wave vector $\boldsymbol{q}$ *into* action with wave vector $\boldsymbol{k}$. Upon integration over ω, both Σ and σ include effects of inelastic scattering via the argument $\mathsf{H}(\boldsymbol{x},\tau\boldsymbol{q},t)-\mathsf{H}(\boldsymbol{x},\boldsymbol{k},t)$ in the correlation function R_{ij}. Note that the slowly varying drift $\boldsymbol{U}(\boldsymbol{x},t)$ also enters parametrically in the scattering through $\mathsf{H}(\boldsymbol{x},\boldsymbol{k},t)$.

However, when the power spectrum is δ-correlated in frequency $R(\boldsymbol{Q}) = R(\boldsymbol{q})\delta(\omega)$, i.e. when the random field $\delta\boldsymbol{U}$ is slowly varying in time, the resulting terms $\delta(\tau\mathsf{H}(\boldsymbol{x},\tau\boldsymbol{q},t)-\mathsf{H}(\boldsymbol{x},\boldsymbol{k},t))$ (in $\Sigma(\boldsymbol{x},\boldsymbol{k},t)$) and $\delta(\tau\mathsf{H}(\boldsymbol{x},\boldsymbol{q},t)-\mathsf{H}(\boldsymbol{x},\boldsymbol{k},t))$ (in $\sigma(\boldsymbol{q},\boldsymbol{k},\boldsymbol{x},t)$) imply that we can consider the independent transport of waves at a fixed frequency $\omega_0 \equiv \mathsf{H}(\boldsymbol{x},\boldsymbol{k},t)$. Even if all waves have frequency ω_0, waves of different wave vectors may nevertheless interact, giving rise to wave number conversion and Doppler effects.

5. Results and discussion

In addition to treating scattering from surface flows containing two explicit length scales, we have further assumed that the amplitude of $\delta\boldsymbol{U}$ scales as ε^β with $\beta = 1/2$: the random flows are correspondingly weakened as the high frequency limit is taken. Since scattering strength is proportional to the power spectrum of the random flows and is quadratic in $\delta\boldsymbol{U}$, heuristically, the mean free path $\ell_{\mathrm{mfp}} \sim c_{\mathrm{g}}(k)/\Sigma(k)\varepsilon^{1-2\beta}$. For $\beta > 1/2$, the scattering is too weak and the mean free path diverges. In this limit, waves are nearly freely propagating and can be described by the slowly varying flows alone, or WKB theory. If $\beta < 1/2$, $\ell_{\mathrm{mfp}} \to 0$ and the scattering becomes so frequent that over a propagation distance of O(1), the large number of scatterings may lead to diffusive (cf. Section 5.4) behavior [26]. Therefore, only random flows that have the scaling $\beta = 1/2$ contribute to the wave transport regime. Moreover, wave localization phenomena are precluded when $\beta > 0$, even in the limit of time-independent $\delta\boldsymbol{U}$. In a two-dimensional random environment, the localization length over which wave diffusion is inhibited is approximately [26]

$$\ell_{\mathrm{loc}} \sim \ell_{\mathrm{mfp}} \exp(\varepsilon^{-1}k\ell_{\mathrm{mfp}}) \sim \varepsilon^{1-2\beta}\exp(\varepsilon^{-2\beta}). \tag{38}$$

As long as the random potential is scaled weaker ($\beta > 0$), $\ell_{\rm loc} \to \infty$, and strong localization will not take hold. In the following subsections, we systematically discuss the salient features of water wave transport contained in Eq. (34) and derive wave diffusion for propagation distances $\gtrsim \mathrm{O}(1)$.

5.1. Slowly varying drift: $\boldsymbol{U}(\boldsymbol{x}, t) \neq 0$, $\delta \boldsymbol{U} = 0$

First consider the case where surface flows vary only on scales much larger than the longest wavelength $2\pi/k$ considered, i.e. $\delta\boldsymbol{U} = 0$. The left-hand side of Eq. (34) represents wave action transport over slowly varying drift and may describe short wavelength modes propagating over flows generated by underlying long surface waves.

The nonscattering terms of the transport equation (34) is equivalent to the results obtained by ray theory (WKB expansion) and conservation of wave action (CWA) [1–6]. Assume the WKB expansion [35,36]

$$\eta_\varepsilon = A_\eta(\boldsymbol{x}, t)\, \mathrm{e}^{\mathrm{i}S(\boldsymbol{X},t)/\varepsilon} \quad \text{and} \quad \varphi_\varepsilon = A_\varphi(\boldsymbol{x}, t)\, \mathrm{e}^{\mathrm{i}S(\boldsymbol{X},t)/\varepsilon}, \tag{39}$$

with smoothly varying A_η and A_φ. Upon using the above *ansatz* in Eq. (13) and setting $\varepsilon \to 0$, we have $a(\boldsymbol{x}, \boldsymbol{k}, t) = |A|^2(\boldsymbol{x}, t)\delta(\boldsymbol{k} - \nabla_{\boldsymbol{x}} S(\boldsymbol{x}, t))$ where $|A|^2 = 2\alpha(k)|A_\varphi|^2 = 2\alpha^{-1}(k)|A_\eta|^2$. Substitution of this expression for $a(\boldsymbol{x}, \boldsymbol{k}, t)$ into Eq. (34), we obtain the following possible equations for $S(\boldsymbol{x}, t)$ and $|A|^2(\boldsymbol{x}, t)$

$$\partial_t S + \mathsf{H}(\boldsymbol{x}, \nabla_{\boldsymbol{x}} S, t) = 0, \qquad \partial_t |A|^2(\boldsymbol{x}, t) + \nabla_{\boldsymbol{x}} \cdot (|A|^2 \nabla_{\boldsymbol{k}} \mathsf{H}(\boldsymbol{x}, \nabla_{\boldsymbol{x}} S, t)) = 0. \tag{40}$$

The first equation is the eikonal equation, while the second equation is the wave action amplitude equation. Recalling that $|A_\eta|^2 = \alpha(k)|A|^2/2$, we obtain the following transport equation for the height amplitude:

$$\partial_t \left(\frac{|A_\eta|^2}{\alpha(\nabla_{\boldsymbol{x}} S)} \right) + \nabla_{\boldsymbol{x}} \cdot \left(\frac{|A_\eta|^2}{\alpha(\nabla_{\boldsymbol{x}} S)} \nabla_{\boldsymbol{k}} \mathsf{H}(\boldsymbol{x}, \nabla_{\boldsymbol{x}} S) \right) = 0. \tag{41}$$

Eq. (41) is the same as Eq. (8) of [5], except that his $\bar{\Omega}$ is replaced here by α owing to our inclusion of surface tension.

Wave action conservation can be understood by noting that

$$\frac{\mathrm{d}}{\mathrm{d}t} a(X(t), K(t), t) = 0, \tag{42}$$

where the characteristics $(X(t), K(t))$ satisfy Hamilton's equations

$$\frac{\mathrm{d}X(t)}{\mathrm{d}t} = \nabla_{\boldsymbol{k}} \mathsf{H}(X(t), K(t)), \qquad \frac{\mathrm{d}K(t)}{\mathrm{d}t} = -\nabla_{\boldsymbol{x}} \mathsf{H}(X(t), K(t)). \tag{43}$$

Here, $X(t)$ and $K(t)$ are the position and wave number of the waves. The solutions to the ordinary differential equation (43) are the characteristic curves used to solve Eq. (40) [37].

5.2. Correlation functions and conservation laws

Now consider the case where $\delta\boldsymbol{U} \neq 0$. The scattering rates defined by Eq. (35) depend upon the precise form of the random flow correlation R_{ij}. There are actually six additional terms in the calculation of σ and Σ which vanish because

$$\sum_{j=1}^{2} R_{ij}(\boldsymbol{Q}) q_j = 0, \quad \text{for } i = 1, 2. \tag{44}$$

To prove relationship (44) we consider the *three-dimensional* and incompressibility properties of $\delta\boldsymbol{U}(\boldsymbol{x}, z, t) = \delta\boldsymbol{U}(\boldsymbol{X}, z)$. If $\delta U_z(\boldsymbol{K}, k_z)$ and $\delta U_z(\boldsymbol{K}, -k_z)$ have the same probability distribution; thus,

$$\langle \delta U_i(\boldsymbol{P}, p_z) \delta U_z(\boldsymbol{K}, k_z) \rangle = \langle \delta U_i(\boldsymbol{P}, p_z) \delta U_z(\boldsymbol{K}, -k_z) \rangle, \tag{45}$$

and

$$\sum_{j=1}^{2}\delta(\boldsymbol{P}+\boldsymbol{K})R_{ij}(\boldsymbol{K})k_j=\sum_{j=1}^{2}\langle\delta U_i(\boldsymbol{P},z{=}0)\delta U_j(\boldsymbol{K},z{=}0)k_j\rangle=\sum_{j=1}^{2}\left\langle\delta U_i(\boldsymbol{P},z=0)\int_{-\infty}^{\infty}\mathrm{d}k_z\,\delta U_j(\boldsymbol{K},k_z)k_j\right\rangle$$
$$=-\int_{-\infty}^{\infty}\langle\delta U_i(\boldsymbol{P},0)\delta U_z(\boldsymbol{K},k_z)\rangle k_z\,\mathrm{d}k_z=0,$$

where we have invoked the a Fourier transform in the z-direction, incompressibility, and Eq. (45), respectively. This result requires the correlation function to be transverse:

$$R_{ij}(|\boldsymbol{Q}|)=R(q,\omega_q)\left[\delta_{ij}-\frac{q_iq_j}{q^2}\right], \tag{46}$$

where $R(q,\omega_q)$ is a scalar function. This transverse nature is the same tensoral structure that would arise for a incompressible two-dimensional fluid and is expected since we considered an infinite layer of fluid of fixed depth h [38]. The correlation kernels in the scattering integrals can now be written as

$$q_iR_{ij}(|\tau\boldsymbol{Q}-\boldsymbol{K}|)k_j=R(|\tau\boldsymbol{Q}-\boldsymbol{K}|)\left[\boldsymbol{q}\cdot\boldsymbol{k}-\frac{\boldsymbol{q}\cdot(\tau\boldsymbol{q}-\boldsymbol{k})\boldsymbol{k}\cdot(\tau\boldsymbol{q}-\boldsymbol{k})}{|\tau\boldsymbol{q}-\boldsymbol{k}|^2}\right]=\tau\frac{R(|\tau\boldsymbol{Q}-\boldsymbol{K}|)}{|\tau\boldsymbol{q}-\boldsymbol{k}|^2}q^2k^2\sin^2\theta, \tag{47}$$

where θ denotes the angle between $\boldsymbol{q}$ and $\boldsymbol{k}$. The scattering must also satisfy the support of the δ-functions; for $\boldsymbol{U}(\boldsymbol{X})=0$ only $|\boldsymbol{q}|=|\boldsymbol{k}|$ satisfy the δ-function constraints. In the presence of slowly varying drift, the evolution of $a(\boldsymbol{X},|\boldsymbol{K}|\neq|\boldsymbol{Q}|)$ can "Doppler" couple to that of $a(\boldsymbol{X},\boldsymbol{Q})$.

It is straightforward to show from the explicit expressions (35) that

$$\Sigma(\boldsymbol{x},\boldsymbol{k},t)=\int\mathrm{d}\boldsymbol{q}\,\sigma(\boldsymbol{x},\boldsymbol{q},\boldsymbol{k},t). \tag{48}$$

This relation indicates that the scattering operator on the right-hand side of Eq. (34) is conservative: Integrating over the whole phase space yields

$$\frac{\mathrm{d}}{\mathrm{d}t}\int_{\boldsymbol{x}}\int_{\boldsymbol{k}}a(\boldsymbol{x},\boldsymbol{k},t)=0. \tag{49}$$

Eq. (49) is the generalization of CWA to include scattering of action from highly oscillating random flows $\delta\boldsymbol{U}(\boldsymbol{X}/\varepsilon)$. Although $a(\boldsymbol{x},\boldsymbol{k},t)$ is conserved, that the total water wave energy $E(\boldsymbol{x},\boldsymbol{k},t)=\Omega(\boldsymbol{k})a(\boldsymbol{x},\boldsymbol{k},t)$ is not conserved is easy to show if $\boldsymbol{U}(\boldsymbol{x})$ is small enough such that the δ-function in the $\sigma(\boldsymbol{q},\boldsymbol{x},\boldsymbol{k},t)$ integral is triggered only when $\tau=+1$. Since $\mathsf{H}(\boldsymbol{x},\boldsymbol{k},t)a(\boldsymbol{x},\boldsymbol{k},t)$ is conserved (as can be seen from Eq. (34)),

$$\frac{\mathrm{d}}{\mathrm{d}t}E=-\frac{\mathrm{d}}{\mathrm{d}t}\int_{\boldsymbol{x}}\int_{\boldsymbol{k}}\boldsymbol{k}\cdot\boldsymbol{U}(\boldsymbol{x},t)\,a(\boldsymbol{x},\boldsymbol{k},t)\neq0. \tag{50}$$

This nonconservation results from the energy that is exchanged between waves and the underlying flow. When $\boldsymbol{U}$ is large enough for Doppler coupling ($\tau=-1$), an additional term arises and neither $\mathsf{H}(\boldsymbol{x},\boldsymbol{k},t)a(\boldsymbol{x},\boldsymbol{k},t)$ nor $E(\boldsymbol{x},\boldsymbol{k},t)$ are conserved.

5.3. Doppler-coupled scattering

For simplicity, we only discuss here time-independent $\delta\boldsymbol{U}$, nonetheless, the transport equation (34) accommodates a rich variety of behaviors. All wave interactions with the underlying flow are thus elastic, and we need only consider a single fixed wave frequency ω_0 and evaluate the support of $\delta(\tau\mathsf{H}(\boldsymbol{x},\tau\boldsymbol{q},t)-\mathsf{H}(\boldsymbol{x},\boldsymbol{k},t))$ (for $\Sigma(\boldsymbol{x},\boldsymbol{k},t)$) and $\delta(\tau\mathsf{H}(\boldsymbol{x},\boldsymbol{q},t)-\mathsf{H}(\boldsymbol{x},\boldsymbol{k},t))$ (for $\sigma(\boldsymbol{x},\boldsymbol{q},\boldsymbol{k},t)$).

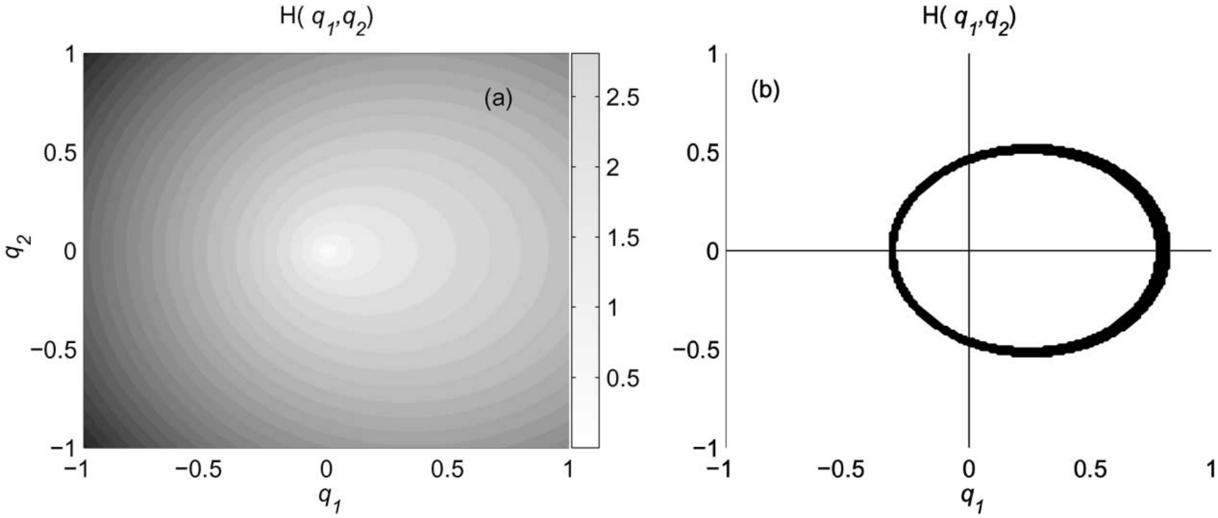

Fig. 2. (a) Contour plot of $\mathsf{H}(\boldsymbol{q})$. Each grayscale corresponds to a different constant value of $\mathsf{H}(\boldsymbol{q}) = \mathsf{H}(\boldsymbol{k}) \equiv \omega_0$. (b) The band of $\boldsymbol{q}$ that satisfies $0.625 < \omega_0 < 0.6625$. Wave vectors $\boldsymbol{q}$ and $\boldsymbol{k}$ that lie in this band can couple $a(\boldsymbol{x}, \boldsymbol{k}, t)$ to $a(\boldsymbol{x}, \boldsymbol{q}, t)$ via wave scattering.

Consider action contained in water waves of fixed wave vector $\boldsymbol{k}$. When $\boldsymbol{U}(\boldsymbol{x}) = 0$, only $\tau = +1$ terms contribute to the integration over $\boldsymbol{q}$ as long as $|\boldsymbol{q}| = |\boldsymbol{k}|$. In this case, we can define the angle $\boldsymbol{q} \cdot \boldsymbol{k} = k^2 \cos\theta$ and reduce the cross-sections to single angular integrals over

$$q_i R_{ij}(|\boldsymbol{q} - \boldsymbol{k}|) q_j = R\left(\left|2k \sin\frac{\theta}{2}\right|\right) \frac{k^2}{4} \frac{\sin^2\theta}{\sin^2\theta/2}, \qquad \tau = +1. \tag{51}$$

Assuming $R(|\boldsymbol{q}|)$ is monotonically decreasing, the most important contribution to the scattering occurs when $\boldsymbol{q}$ and $\boldsymbol{k}$ are collinear.

When $\boldsymbol{U}(\boldsymbol{x}) \neq 0$, and $\tau = +1$, the sets of $\boldsymbol{q}$ which satisfy $\Omega(\boldsymbol{q}) + \boldsymbol{U}(\boldsymbol{x}) \cdot \boldsymbol{q} = \Omega(\boldsymbol{k}) + \boldsymbol{U}(\boldsymbol{x}) \cdot \boldsymbol{k} \equiv \omega_0$ trace out closed ellipse-like curves and are shown in the contour plots of $\mathsf{H}(\boldsymbol{q})$ in Fig. 2(a). The parameters used are $\boldsymbol{U}(\boldsymbol{x}) \cdot \boldsymbol{k}_1 = -0.5k_1$ and $h = \infty$ (the $-\boldsymbol{k}_1, -\boldsymbol{q}_1$ directions are defined by the direction of $\boldsymbol{U}(\boldsymbol{x})$). Each grayscale corresponds to a curve defined by fixed $\mathsf{H}(\boldsymbol{k}) = \omega_0$. All wave vectors $\boldsymbol{q}$ in each contour contribute to the integration in the expressions for $\Sigma(\boldsymbol{k})$ and $\mathsf{H}(\boldsymbol{q}, \boldsymbol{k})$. Thus, slowly varying drift can induce an indirect Doppler coupling between waves with different wave numbers, with the most drastic coupling occurring at the two far ends of a particular oval curve. For example, in Fig. 2(b), the dark band denotes $\boldsymbol{q}$ such that $\mathsf{H}(\boldsymbol{q}) = \omega_0$ when $0.625 < \omega_0 < 0.6625$. The wave vectors $\boldsymbol{q} \approx (-0.3, 0)$ and $\boldsymbol{q} \approx (0.8, 0)$ are two of many that contribute to the scattering terms. Therefore, the evolution of $a(\boldsymbol{x}, \boldsymbol{k} \approx (-0.3, 0), t)$ also depends on $a(\boldsymbol{x}, \boldsymbol{q} \approx (0.8, 0), t)$ via the second term on the right-hand side of Eq. (34).

Provided $\boldsymbol{U}(\boldsymbol{x})$ is sufficiently large, the $\tau = -1$ terms can also contribute to scattering. The dissipative scattering rate $\Sigma(\boldsymbol{k})a(\boldsymbol{x}, \boldsymbol{k}, t)$ will only change quantitatively since additional $\boldsymbol{q}$'s will contribute to $\Sigma(\boldsymbol{k})$. However, this decay process depends only on $\boldsymbol{k}$ and is not coupled to $a(\boldsymbol{x}, |\boldsymbol{q}| \neq |\boldsymbol{k}|, t)$. Wave vectors $\boldsymbol{q}$ that satisfy the δ-function in the $\sigma(\boldsymbol{q}, \boldsymbol{x}, \boldsymbol{k}, t)a(\boldsymbol{x}, \boldsymbol{q}, t)$ term will, as when $\tau = +1$, lead to indirect Doppler coupling. This occurs when $\mathsf{H}(\boldsymbol{q}, \boldsymbol{x}, \boldsymbol{k}, t) = -\omega_0$ and, as we shall see, allows Doppler coupling of waves with more widely varying wavelengths than compared to the $\tau = +1$ case. If $\tau = -1$ terms arise, the drift frame energy $a(\boldsymbol{x}, \boldsymbol{k}, t)\mathsf{H}(\boldsymbol{x}, \boldsymbol{k})$ is no longer conserved. Fig. 3(a) plots $\mathsf{H}(q_1, q_2 = 0)$ for $U(\boldsymbol{x}) = 1 < \sqrt{2}, U(\boldsymbol{x}) = \sqrt{2}$, and $U(\boldsymbol{x}) = 1.6 > \sqrt{2}$. Since ω_0 and $\mathsf{H}(\boldsymbol{q})$ are identical functions, $-\omega_0$ can take on values below the upper dotted line ($\omega_0 \lesssim 0.22$ for $U = 1.6$). Therefore, coupling for $\tau = -1$ and $q_2 = 0$ occurs for values of $-\omega_0$ between the dotted lines. Depending upon

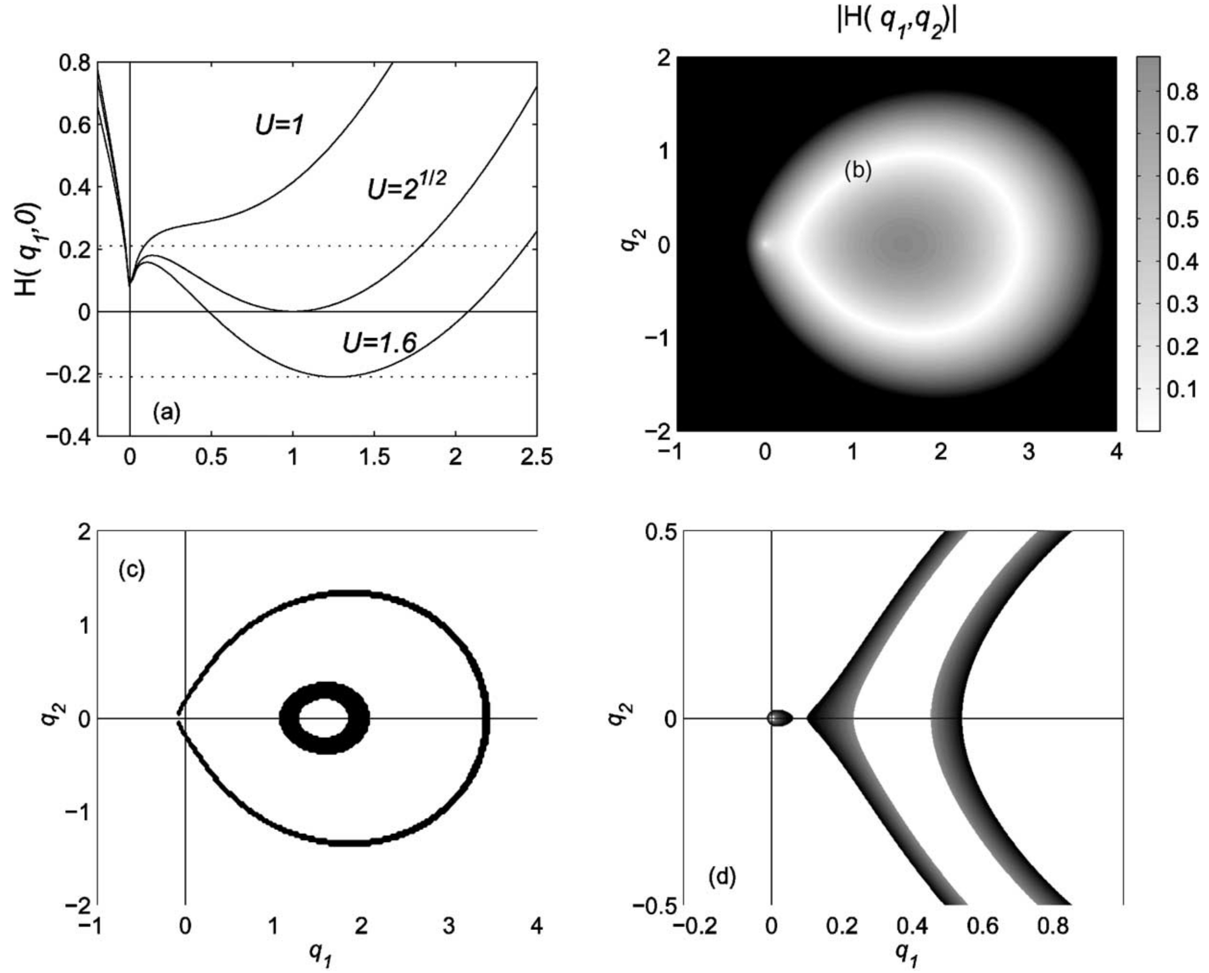

Fig. 3. Conditions for Doppler coupling when $\tau = -1$. (a) Plot of $\mathsf{H}(q_1, q_2 = 0; h = \infty)$ for $U = 1$, $U = \sqrt{2}$, and $U = 1.6$. Only for $U > \sqrt{2}$ does $\mathsf{H}(q_1, q_2 = 0; h = \infty) < 0$. (b) Contour plot of $|\mathsf{H}(\boldsymbol{q})|$. Each grayscale corresponds to a different constant value of $\mathsf{H}(\boldsymbol{q}) = \mathsf{H}(\boldsymbol{k}) \equiv -\omega_0$. (c) The bands of $\boldsymbol{q}$ satisfying $0.414 < -\omega_0 < 0.468$. (d) An expanded view of the coupling bands for $0.0756 < -\omega_0 < 0.1368$. Note that wave numbers of very small modulus can couple with wave numbers of significantly larger modulus.

the value of ω_0, coupling can occur at two or four different points $\boldsymbol{q} = (q_1, 0)$. Fig. 3(b) shows a contour plot of $\mathsf{H}(\boldsymbol{q})|$ as a function of (q_1, q_2). A level set lying between the dotted lines in (a) will slice out two bands; one band corresponds to all values of $\boldsymbol{k}$ that couple to $\boldsymbol{q}$ lying in the associated second band. Two bands determined by the interval $0.414 < -\omega_0 < 0.468$ are shown in Fig. 3(c). For any $\boldsymbol{k}$ lying in the inner band of Fig. 3(c), all $\boldsymbol{q}$ lying in the outer band will contribute to Doppler coupling for $\tau = -1$, and vice versa. As $-\omega_0$ is increased, the inner (outer) band decreases (increases) in size, with the central band vanishing when $-\omega_0$ approaches the upper dotted line in (a) where the $\tau = -1$ coupling evaporates. If $-\omega_0$ is decreased, the two bands merge, then disappear as $-\omega_0$ reaches the lower limit. Fig. 3(d) is an expanded view of the two bands for small $0.0756 < -\omega_0 < 0.1368$. Note that a small island of $\boldsymbol{q}$ or $\boldsymbol{k}$ appears for very small wave vectors. The water wave scattering represented by $\sigma(\boldsymbol{q}, \boldsymbol{k})$ can therefore couple very long wavelength modes with very short wavelength modes (the two larger bands to the right in Fig. 3(d)). However, the strength of this coupling is still determined by the magnitude of $q_i R_{ij}(|\boldsymbol{q} - \boldsymbol{k}|)k_j$, which may be small for large $|\boldsymbol{q} - \boldsymbol{k}|$. If $\delta \boldsymbol{U}(t/\varepsilon)$ is time-dependent, the oval curves discussed in Figs. 2 and 3 will be broadened as interactions among waves of different frequencies arise. Not only do waves of different wave vectors interact through the $\delta\boldsymbol{U}$, within each oval curve, but waves of different frequency interact by virtue of the time dependence of $\delta\boldsymbol{U}$, coupling different level sets.

The depth dependence of Doppler coupling will be relevant when $hq, hk \lesssim 1$ where q and k are the magnitudes of the wave vectors of two Doppler-coupled waves. For $\tau = +1$, finite depth reduces the ellipticity of the coupling bands, resulting in weaker Doppler effects. Since the water wave phase velocity decreases with h, a finite depth will also reduce the critical $U(\boldsymbol{x})$ required for $\tau = -1$ Doppler coupling. For small $U(\boldsymbol{x})$, it is clear that the δ-functions associated with the $\tau = -1$ terms in $\sigma(\boldsymbol{q}, \boldsymbol{k})$ are first triggered when the $\boldsymbol{q}$ and $\boldsymbol{k}$ are antiparallel, $\boldsymbol{U} \cdot \boldsymbol{k} = -k|\boldsymbol{U}|, \boldsymbol{U} \cdot \boldsymbol{q} = +q|\boldsymbol{U}|$. Fig. 4(a) shows the phase velocity for various depths h. In order for $\tau = -1$ to contribute to scattering, $U \geq c_\phi(k; h)$. For $U \approx 1.6$, this condition holds in the $h = \infty$ case for $0.5 \lesssim k \lesssim 2$ (the dashed region of $c_\phi(k, \infty)$). Recall that our starting equations (system (4)) are valid only in the small Froude number limit. However, for water waves propagating over infinite depth, $\tau = -1$ coupling requires $U > U_{\min} = \min_k\{c_\phi(k)\}$, with $c_\phi(k_{\min}) \simeq 22\,\text{cm/s}$. Therefore, in such "supersonic" cases, where $\tau = -1$ is relevant, our treatment is accurate only at wave vectors k^* such that $U \ll c_\phi(k^*; h)$, e.g. the thick solid portion of $c_\phi(k; \infty)$ in Fig. 4(a). For $U \gtrsim U_{\min}$, the $\tau = -1$ term can couple wave vectors $q \approx 0 \ll k_{\min}$ with $k \approx 2 - 3 \gg k_{\min}$. The rich $\tau = -1$ Doppler coupling displayed in Fig. 3 is peculiar to water waves with a dispersion relation $\mathsf{H}(\boldsymbol{q})$ that behaves as $q^{3/2}$, $\boldsymbol{U} \cdot \boldsymbol{q}$, or $q^{1/2}$ depending on the wavelength. Doppler coupling in water wave propagation is very different from that arising in acoustic wave propagation in an incompressible, randomly flowing fluid [21,22,39] where $\mathsf{H}(\boldsymbol{q}) = c_s|\boldsymbol{q}|$. An additional Doppler coupling analogous to the $\tau = -1$ coupling for water waves arises only for supersonic random flows when $U(\boldsymbol{x}) \geq c_s$, independent of q. In such instances, compressibility effects must also be considered.

Fig. 4(b) plots the minimum drift velocity $U_{\min}(h)$ where $\tau = -1$ Doppler coupling first occurs at any wave vector. The wave vector at which coupling first occurs is also shown by the dashed curve. For shallow water, $h \ll \sqrt{3}$, $U_{\min}(h) \propto \sqrt{h}$ and very long wavelengths couple first (small $k(U_{\min})$). For depths $h > \sqrt{3}$ ($\sim 3\,\text{cm}$ for water), the minimum drift required quickly increases to $U^*(\infty) = \sqrt{2}$, while the initial coupling occurs at increasing wave vectors until at infinite depth, where the first wave vector to Doppler couple approaches $k \to 1$ (in water, this corresponds to wavelengths of $\sim 6.3\,\text{cm}$). The conditions for $\tau = -1$ Doppler coupling outlined in Figs. 2 and 3 apply to both $\Sigma(\boldsymbol{k})$ and $\sigma(\boldsymbol{q}, \boldsymbol{k})$, with the proviso that $\boldsymbol{q}$ and $\boldsymbol{k}$ are parallel for $\Sigma(\boldsymbol{k})$ and antiparallel for $\sigma(\boldsymbol{q}, \boldsymbol{k})$. However, even when $U < U_{\min}$ such that only $\tau = +1$ applies, the set of $\boldsymbol{q}$ corresponding to a constant

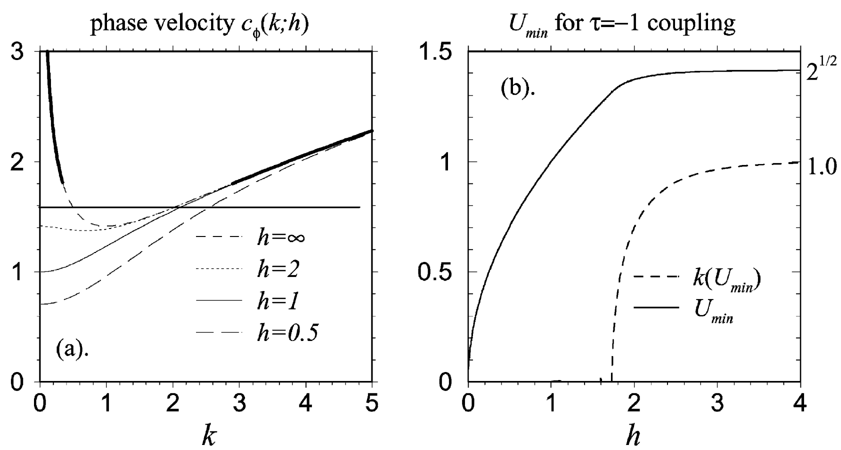

Fig. 4. $U > c_\phi(k)$ is required for $\tau = -1$ coupling. (a) The phase velocity $c_\phi(k)$ for various depths h. The velocity shown by the solid horizontal line $U \approx 1.6 > c_\phi(k; h = \infty)$ for $0.5 \lesssim k \lesssim 2$. (b) The minimum $U_{\min}(h)$ required for existence of $\tau = -1$ coupling at any wave vector k, and the wave vector $k(U_{\min})$ at which this first happens.

value of $\mathsf{H}(\boldsymbol{k}) = \omega_0$, traces out a noncircular curve. There is Doppler coupling between wave numbers $q \neq k$ as long as $U \neq 0$.

5.4. Surface wave diffusion

We now consider the radiative transfer equation (34) over propagation distances long compared to the mean free path $\ell_{\rm mfp}$. Imposing an additional rescaling and measuring all distances in terms of the mean free path, we introduce another scaling ϵ^{-1}, proportional to the number of mean free paths traveled. Since $\beta = 1/2$, transport of wave action prevails when $\mathrm{O}(\varepsilon) < |\boldsymbol{x}| \sim \mathrm{O}(1)$, while diffusion may arise when $\mathrm{O}(\epsilon^{-1}) \sim |\boldsymbol{x}| < \ell_{\rm loc}$.

In the special case of time-independent $\delta\boldsymbol{U}$, waves of each frequency satisfy Eq. (34) independently. To derive a diffusion equation for waves of frequency ω_0, we assume for simplicity that $\boldsymbol{U}$ is constant and small such that $\omega_0 + \mathsf{H}(\boldsymbol{x}, \boldsymbol{q}) \neq 0$ (the $\tau = -1$ terms are never triggered by the δ-functions). Expanding all quantities in the transport equation (34) in powers of ϵ, one can find

$$\dot{a} + \bar{\boldsymbol{U}} \cdot \nabla_{\boldsymbol{x}} a - \nabla_{\boldsymbol{x}} \cdot \boldsymbol{D} \cdot \nabla_{\boldsymbol{x}} a = 0. \qquad (52)$$

The effective drift $\bar{\boldsymbol{U}}$ is given by

$$\bar{\boldsymbol{U}} = \frac{\int_{\boldsymbol{k}} \nabla_{\boldsymbol{k}} \mathsf{H}(\boldsymbol{k}) \delta(\boldsymbol{k} \cdot \boldsymbol{U} + \Omega(\boldsymbol{k}) - \omega_0)}{\int_{\boldsymbol{k}} \delta(\boldsymbol{k} \cdot \boldsymbol{U} + \Omega(\boldsymbol{k}) - \omega_0)}. \qquad (53)$$

For $\boldsymbol{U} = 0$, $h = \infty$ and $\omega_\infty(\boldsymbol{k}) = \sqrt{k^3 + k}$, the isotropic diffusion tensor becomes

$$\boldsymbol{D} = \frac{1}{\Sigma(k) V_{\omega_0}} \int_{\boldsymbol{Q}} |\nabla_{\boldsymbol{Q}} \Omega_\infty(\boldsymbol{q})|^2 \hat{\boldsymbol{q}} \hat{\boldsymbol{q}}^{\mathrm{T}} \delta(\Omega_\infty(\boldsymbol{q}) - \omega_0) = \frac{c_{\rm g}^2(k)}{2\Sigma(k)} \boldsymbol{I}, \qquad (54)$$

where $V_{\omega_0} = \int_{\boldsymbol{k}} \delta(\mathsf{H}(\boldsymbol{k}) - \omega_0)$ and $\boldsymbol{I}$ is the 2×2 identity matrix. Thus, the diffusion equation for $a(\boldsymbol{x}, t)$ assumes the standard form [26]

$$\dot{a} - \frac{c_{\rm g}^2(k)}{2\Sigma(k)} \Delta a = 0. \qquad (55)$$

Recall that dissipation may allow for transport, but if $\nu k^2 \not\ll \varepsilon^2 c_{\rm g}(k)$ (compare Eq. (25)), diffusion can be precluded. For one meter waves, the possibility of diffusion requires $\varepsilon \ll 8 \times 10^{-3}$. Diffusion exists strictly in the limit of time-independent $\delta\boldsymbol{U}$; for time-varying $\delta\boldsymbol{U}$, wave action dynamics becomes more complicated due to random flow-mediated energy exchange among the waves.

6. Summary and conclusions

We have used the Wigner distribution to derive the transport equations for water wave propagation over a spatially random drift composed of a slowly varying part $\boldsymbol{U}(\boldsymbol{X})$, and a rapidly varying part $\sqrt{\varepsilon}\delta\boldsymbol{U}(\boldsymbol{X}/\varepsilon)$. The slowly varying part determines the characteristics on which the waves propagate. We recover the standard result obtained from WKB theory: conservation of wave action. Provided $R_{ij}(\boldsymbol{Q}) q_j = 0$, we extend CWA to include wave scattering from correlations R_{ij} of the rapidly varying (both in space and time) random flow. Evolution equations for the nonconserved wave intensity and energy density can be readily obtained from Eq. (34). Moreover, conservation of drift frame energy $a(\boldsymbol{x}, \boldsymbol{k}, t)\mathsf{H}(\boldsymbol{x}, \boldsymbol{k}, t)$ requires small $U < U_{\min}$ and absence of $\tau = -1$ contributions to scattering.

Explicit expressions for the scattering rates $\Sigma(\boldsymbol{x}, \boldsymbol{k}, t)$ and $\sigma(\boldsymbol{q}, \boldsymbol{x}, \boldsymbol{k}, t)$ are given in Eq. (35). Even in the limiting case of time-independent $\delta\boldsymbol{U}$, wave number conversion can arise for a fixed frequency. For fixed $\omega_0 = \mathsf{H}(\boldsymbol{k})$, we find the set of $\boldsymbol{q}$ such that the δ-functions in Eq. (35) are supported. This set of $\boldsymbol{q}$ indicates the wave vectors of the background surface flow that can mediate Doppler coupling of the water waves. Although widely varying wave numbers can Doppler couple, supported by the δ-function constraints, particularly for $\tau = -1$, the correlation $R_{ij}(|\boldsymbol{q}-\boldsymbol{k}|)$ also decreases for large $|\boldsymbol{q}-\boldsymbol{k}|$. For long times, multiple weak scattering nonetheless exchanges action among disparate wave numbers within the transport regime. Our collective results, including water wave action diffusion, may provide a model for describing linear ocean wave propagation over random flows of different length scales. The scattering terms in Eq. (34) also provide a means to correlate sea surface wave spectra to statistics R_{ij} of finer scale random flows.

The recent extension by [5] of CWA to include rotational flows also suggests that an explicit consideration of velocity and pressure can be used to generalize the present study to include rotational random flows. Other feasible extensions include more detailed analyses of the energy and action cascade arising from a time-dependent $\delta\boldsymbol{U}$.

Acknowledgements

The authors thank A. Balk, M. Moscoso, G. Papanicolaou, L. Ryzhik, and I. Smolyarenko for helpful comments and discussion. GB was supported by AFOSR Grant 49620-98-1-0211 and NSF Grant DMS-9709320. TC was supported by NSF Grant DMS-9804370.

Appendix A. Derivation of the transport equation

Some of the steps in the derivation of Eq. (34) are outlined here. By taking the time derivative of W_{ij} in Eq. (14) and using the definition (17) for $\dot{\psi}$, we obtain

$$\begin{aligned} 0 &= (2\pi\varepsilon)^3 \mathrm{i} W_{i\ell}(\boldsymbol{P},\boldsymbol{K}) L^*_{\ell j}\left(-\frac{\boldsymbol{K}}{\varepsilon}-\frac{\boldsymbol{P}}{2}\right) - (2\pi\varepsilon)^3 \mathrm{i} L_{i\ell}\left(-\frac{\boldsymbol{K}}{\varepsilon}+\frac{\boldsymbol{P}}{2}\right) W_{\ell j}(\boldsymbol{P},\boldsymbol{K}) \\ &+\mathrm{i}\int_{\boldsymbol{Q}} \boldsymbol{U}(\boldsymbol{Q})\cdot\left(-\frac{\boldsymbol{k}}{\varepsilon}+\frac{\boldsymbol{p}}{2}-\boldsymbol{q}\delta_{i2}\right)\psi_i\left(-\frac{\boldsymbol{K}}{\varepsilon}+\frac{\boldsymbol{P}}{2}-\boldsymbol{Q}\right)\psi_j^*\left(-\frac{\boldsymbol{K}}{\varepsilon}-\frac{\boldsymbol{P}}{2}\right) \\ &-\mathrm{i}\int_{\boldsymbol{Q}} \boldsymbol{U}^*(\boldsymbol{Q})\cdot\left(-\frac{\boldsymbol{k}}{\varepsilon}-\frac{\boldsymbol{p}}{2}-\boldsymbol{q}\delta_{j2}\right)\psi_i\left(-\frac{\boldsymbol{K}}{\varepsilon}+\frac{\boldsymbol{P}}{2}\right)\psi_j^*\left(-\frac{\boldsymbol{K}}{\varepsilon}-\frac{\boldsymbol{P}}{2}-\boldsymbol{Q}\right) \\ &+\mathrm{i}\sqrt{\varepsilon}\int_{\boldsymbol{Q}} \delta\boldsymbol{U}(\boldsymbol{Q})\cdot\left(-\frac{\boldsymbol{k}}{\varepsilon}+\frac{\boldsymbol{p}}{2}-\frac{\boldsymbol{q}}{\varepsilon}\delta_{i2}\right)\psi_i\left(-\frac{\boldsymbol{K}}{\varepsilon}+\frac{\boldsymbol{P}}{2}-\frac{\boldsymbol{Q}}{\varepsilon}\right)\psi_j^*\left(-\frac{\boldsymbol{K}}{\varepsilon}-\frac{\boldsymbol{P}}{2}\right) \\ &-\mathrm{i}\sqrt{\varepsilon}\int_{\boldsymbol{Q}} \delta\boldsymbol{U}^*(\boldsymbol{Q})\cdot\left(-\frac{\boldsymbol{k}}{\varepsilon}-\frac{\boldsymbol{p}}{2}-\frac{\boldsymbol{q}}{\varepsilon}\delta_{j2}\right)\psi_i\left(-\frac{\boldsymbol{K}}{\varepsilon}+\frac{\boldsymbol{P}}{2}\right)\psi_j^*\left(-\frac{\boldsymbol{K}}{\varepsilon}-\frac{\boldsymbol{P}}{2}-\frac{\boldsymbol{Q}}{\varepsilon}\right). \end{aligned} \tag{A.1}$$

To rewrite the above expression as a function of W_{ij} only, we relabel appropriately, e.g.

$$-\frac{\boldsymbol{K}}{\varepsilon}-\frac{\boldsymbol{P}}{2} = -\frac{\boldsymbol{K}'}{\varepsilon}-\frac{\boldsymbol{P}'}{2}-\frac{\boldsymbol{K}}{\varepsilon}+\frac{\boldsymbol{P}}{2}-\boldsymbol{Q} = -\frac{\boldsymbol{K}'}{\varepsilon}+\frac{\boldsymbol{P}'}{2}, \tag{A.2}$$

for the third term on the right-hand side of Eq. (A.1). Similarly relabelling for all relevant terms yields the integral equation (19).

The $\mathrm{O}(\varepsilon^{-1/2})$ terms of Eq. (19) determine $\boldsymbol{W}_{1/2}$. Decomposing

$$\boldsymbol{W}_{1/2}(\boldsymbol{P},\boldsymbol{\Xi},\boldsymbol{K}) \equiv \sum_{\tau,\tau'=\pm} a^{(1/2)}_{\tau,\tau'}(\boldsymbol{P},\boldsymbol{\Xi},\boldsymbol{K})\boldsymbol{b}_\tau(\boldsymbol{k}_-)\boldsymbol{b}^\dagger_{\tau'}(\boldsymbol{k}_+), \tag{A.3}$$

and substituting into Eq. (30) we find the coefficients $a^{(1/2)}_{\tau,\tau'}$, where in this case $a^{(1/2)}_{+-}, a^{(1/2)}_{-+} \neq 0$. Due to the nonlocal nature of the third term on the right-hand side of Eq. (30), we must first inverse Fourier transform the slow wave vector variable back to $\boldsymbol{X}$.

To extract the $\mathrm{O}(\varepsilon^0)$ terms from Eq. (19) we need to expand $\boldsymbol{L}$ to order ε^0, the $\boldsymbol{L}_1$ term. Similarly, the terms $\boldsymbol{W}(\boldsymbol{P}-\boldsymbol{Q}, \boldsymbol{\Xi}, \boldsymbol{K} \pm \varepsilon \boldsymbol{Q}/2)$ must be expanded:

$$\boldsymbol{W}\left(\boldsymbol{P}-\boldsymbol{Q}, \boldsymbol{\Xi}, \boldsymbol{K} \pm \tfrac{1}{2}\varepsilon \boldsymbol{Q}\right) = \boldsymbol{W}(\boldsymbol{P}-\boldsymbol{Q}, \boldsymbol{\Xi}, \boldsymbol{K}) \pm \tfrac{1}{2}\varepsilon \boldsymbol{q} \cdot \nabla_{\boldsymbol{k}} \boldsymbol{W}(\boldsymbol{P}-\boldsymbol{Q}, \boldsymbol{\Xi}, \boldsymbol{K}) + \mathrm{O}(\varepsilon^2). \tag{A.4}$$

The $\varepsilon \boldsymbol{q} \cdot \nabla_{\boldsymbol{k}} \boldsymbol{W}(\boldsymbol{P}-\boldsymbol{Q}, \boldsymbol{\Xi}, \boldsymbol{K})$ terms combine with the $-\varepsilon^{-1}\boldsymbol{U}(\boldsymbol{Q}) \cdot \boldsymbol{k}_- + \varepsilon^{-1}\boldsymbol{U}(\boldsymbol{Q}) \cdot \boldsymbol{k}_+$ terms from the third and fourth terms in Eq. (19) to give the third term on the right of Eq. (33). The $\delta \boldsymbol{U}$-dependent, order ε^0 terms (the sixth, seventh, and eighth terms on the right-hand side of Eq. (33)) come from collecting

$$\pm\sqrt{\varepsilon}\delta \boldsymbol{U}(\boldsymbol{Q}) \cdot \left(-\frac{\boldsymbol{k}}{\varepsilon} \pm \frac{\boldsymbol{\xi}}{2\varepsilon}\right)\sqrt{\varepsilon}\boldsymbol{W}_{1/2}\left(\boldsymbol{P}, \boldsymbol{\Xi}-\boldsymbol{Q}, \boldsymbol{K} \pm \frac{\boldsymbol{Q}}{2}\right), \tag{A.5}$$

from the last two terms in Eq. (19). The regularization γ allows certain terms involving $\boldsymbol{W}_{1/2}$ (cf. Eq. (31)) to combine in the form

$$\begin{aligned}&\lim_{\gamma\to 0}\left[\frac{1}{\omega_{k_-} - \omega_{k_+} + \tau' \Omega(\boldsymbol{k}_+) - \tau \Omega(\boldsymbol{k}_-) + \boldsymbol{U}(\boldsymbol{X}) \cdot \boldsymbol{\xi} + 2\mathrm{i}\gamma} - \mathrm{c.c.}\right] \\ &\quad = -2\pi \mathrm{i} \delta\left(\omega_{k_-} - \omega_{k_+} + \tau' \Omega(\boldsymbol{k}_+) - \tau \Omega(\boldsymbol{k}_-) + \boldsymbol{U}(\boldsymbol{X}) \cdot \boldsymbol{\xi}\right).\end{aligned} \tag{A.6}$$

Upon using the *on-shell* relation (27), the ensemble averaged time evolution of the Wigner amplitude $a_\sigma(\boldsymbol{x}, \boldsymbol{k}, t)$ can be succinctly written in the form:

$$\begin{aligned}&\partial_t a_+(\boldsymbol{x}, \boldsymbol{k}, t) + \nabla_{\boldsymbol{k}} \mathsf{H}(\boldsymbol{x}, \boldsymbol{k}, t) \cdot \nabla_{\boldsymbol{x}} a_+(\boldsymbol{x}, \boldsymbol{k}, t) - \nabla_{\boldsymbol{x}} \mathsf{H}(\boldsymbol{x}, \boldsymbol{k}, t) \cdot \nabla_{\boldsymbol{k}} a_+(\boldsymbol{x}, \boldsymbol{k}, t) \\ &\quad = -\Sigma(\boldsymbol{x}, \boldsymbol{k}, t) a_+(\boldsymbol{x}, \boldsymbol{k}, t) + \sum_{\mu=\pm}\int_{\boldsymbol{Q}} \sigma_{+,\mu}(\boldsymbol{x}, \boldsymbol{q}, \boldsymbol{k}, t) a_\mu(\boldsymbol{x}, \boldsymbol{q}, t).\end{aligned} \tag{A.7}$$

Using the form for $\boldsymbol{W}_0$ found from Eq. (23) to find $\boldsymbol{W}_{1/2}$, we substitute into Eq. (33) to find the result (34), the transport equation for one of the diagonal intensities of the Wigner distribution. We have explicitly used eigenbasis orthonormality $\boldsymbol{b}_\tau^\dagger(\boldsymbol{k}) \cdot \boldsymbol{c}_{\tau'}(\boldsymbol{k}) = \boldsymbol{d}_{\tau,\tau'}$ and the fact that $a_-(\boldsymbol{x}, \boldsymbol{k}, t) = a_+(\boldsymbol{x}, -\boldsymbol{k}, t)$.

References

[1] D.H. Peregrine, Interaction of water waves and currents, Adv. Appl. Mech. 16 (1976) 9–117.
[2] I.G. Jonsson, Wave–current interactions, in: B. Le Mehaute, D. Hanes (Eds.), Ocean Engineering Science: The Sea, Wiley/Interscience, New York, 1990, pp. 65–120.
[3] M.S. Longuet-Higgins, R.W. Stewart, The changes in amplitude of short gravity waves on steady non-uniform currents, J. Fluid Mech. 10 (1961) 529–549.
[4] C.C. Mei, The Applied Dynamics of Ocean Surface Waves, Wiley/Interscience, New York, 1979.
[5] B.S. White, Wave action on currents with vorticity, J. Fluid Mech. 386 (1999) 329–344.
[6] G.B. Whitham, Linear & Nonlinear Waves, Wiley/Interscience, New York, 1974.
[7] M. Naciri, C.C. Mei, Evolution of a short surface wave on a very long surface wave of finite amplitude, J. Fluid Mech. 235 (1992) 415–452.
[8] K. Hasselmann, On the mass and momentum transfer between short gravity and larger-scale motions, J. Fluid Mech. 50 (1971) 189–205.
[9] A.L. Fabrikant, .A. Raevsky, Influence of drift flow turbulence on surface gravity-wave propagation, J. Fluid Mech. 262 (1994) 141–156.
[10] E. Cerda, F. Lund, Interaction of surface waves with vorticity in shallow water, Phys. Rev. Lett. 70 (1993) 3896–3899.
[11] T. Chou, S.K. Lucas, H.A. Stone, Capillary wave scattering from a surfactant domain, Phys. Fluids 7 (1995) 1872–1885.
[12] S. Gou, A.F. Messiter, W.W. Schultz, Capillary–gravity waves in a surface tension gradient I: discontinuous change, Phys. Fluids A 5 (1993) 966–972.
[13] T. Chou, D.R. Nelson, Surface wave scattering from nonuniform interfaces, J. Chem. Phys. 101 (1994) 9022–9031.
[14] K.Y. Lee, T. Chou, D.S. Chung, E. Mazur, Direct measurement of the spatial damping of capillary waves at liquid–vapor interfaces, J. Phys. Chem. 97 (1993) 12876–12878.
[15] T. Chou, Band structure of surface flexural-gravity waves along periodic interfaces, J. Fluid Mech. 369 (1998) 333–350.
[16] M. Naciri, C.C. Mei, Bragg scattering of water waves by a doubly periodic seabed, J. Fluid Mech. 192 (1988) 51–74.

[17] M. Gerber, The interaction of deep-gravity waves and an annular current: linear theory, J. Fluid Mech. 248 (1993) 153–172.
[18] K. Trulsen, C.C. Mei, Double reflection of capillary/gravity waves by a non-uniform current: a boundary layer theory, J. Fluid Mech. 251 (1993) 239–271.
[19] J.F. Elter, J.E. Molyneux, The long-distance propagation of shallow water waves over an ocean of random depth, J. Fluid Mech. 53 (1972) 1–15.
[20] P. Kleinert, A field-theoretical treatment of third-sound localization, Phys. Stat. Sol. B 158 (1990) 539–550.
[21] A. Fannjiang, L. Ryzhik, Radiative transfer of sound waves in a random flow: Turbulent scattering and mode-coupling, SIAM J. Appl. Math. 61 (2001) 1545–1577.
[22] M. Howe, Multiple scattering of sound by turbulence and other inhomogeneities, J. Sound Vibration 27 (1973) 455–476.
[23] M.A. Rayevskiy, On the propagation of gravity waves in randomly inhomogeneous nonsteady-state currents, Izvestiya, Atmos. Oceanic Phys. 19 (1983) 475–479.
[24] L.V. Ryzhik, G.C. Papanicolaou, J.B. Keller, Transport equations for elastic and other waves in random media, Wave Motion 24 (1996) 327–370.
[25] K.M. Watson, B.J. West, A transport-equation description of nonlinear ocean surface waves interactions, J. Fluid Mech. 70 (1975) 815–826.
[26] P. Sheng, Introduction to Wave Scattering, Localization, and Mesoscopic Phenomena, Academic Press, New York, 1995.
[27] E. Wigner, On the quantum correction for thermodynamic equilibrium, Phys. Rev. 40 (1932) 742–749.
[28] P.Gérard, P.A. Markowich, N.J. Mauser, F. Poupaud, Homogenization limits and Wigner transforms, Comm. Pure Appl. Math. 50 (1997) 323–380.
[29] L.D. Landau, Fluid Mechanics, Pergamon Press, New York, 1985.
[30] F.S. Henyey, D.B. Creamer, K.B. Dysthe, R.L. Schult, J.A. Wright, The energy and action of small waves riding on large waves, J. Fluid Mech. 189 (1998) 443–462.
[31] G. Bal, A. Fannjiang, G. Papanicolaou, L. Ryzhik, Radiative transport in a periodic structure, J. Stat. Phys. 95 (1999) 479–494.
[32] H. Spohn, Derivation of the transport equation for electrons moving through random impurities, J. Stat. Phys. 17 (1977) 385–412.
[33] L. Erdös, H.T. Yau, Linear Boltzmann equation as scaling limit of quantum Lorentz gas, Adv. Differen. Equations Math. Phys. Contemporary Mathematics 217 (1998) 136–155.
[34] V.E. Zakharov, V.S. L'vov, G. Falkovich, Kolgomorov Spectra of Turbulence I: Wave Turbulence, Springer, Berlin, 1992.
[35] C.M. Bender, S.A. Orszag, Advanced Mathematical Methods for Scientists and Engineers, McGraw-Hill, New York, 1978.
[36] J.B. Keller, Surface Waves on water of non-uniform depth, J. Fluid Mech. 4 (1958) 607–614.
[37] R. Courant, D. Hilbert, Methods of Mathematical Physics, Vol. II, Wiley/Interscience, New York, 1953.
[38] D. Forster, Hydrodynamic Fluctuations, Broken Symmetry, and Correlation Functions, Benjamin, Reading, MA, 1975.
[39] R. Vedantham, J. Hunter, Sound wave propagation through incompressible flows, Wave Motion 26 (1997) 319–328.